Synthesis, Structure, and Electronic Spectroscopy of Neutral, Dinuclear Gold(I) Complexes. Gold(I)–Gold(I) Interactions in Solution and in the Solid State

Ratnavathany Narayanaswamy,[1a] Michelle A. Young,[1a] Erica Parkhurst,[†,1a] Michelle Ouellette,[‡,1a] Margaret E. Kerr,[1a] Douglas M. Ho,[1b,1c] Richard C. Elder,[*,1b] Alice E. Bruce,[*,1a] and Mitchell R. M. Bruce[*,1a]

Departments of Chemistry, University of Maine, Orono, Maine 04469, and University of Cincinnati, Cincinnati, Ohio 45221

Received August 7, 1992

A series of neutral, dinuclear gold(I) complexes containing phosphine and thiolate ligands have been synthesized and characterized by elemental analysis and by ^1H and ^{31}P NMR and UV–visible spectroscopy. Crystal structures of two of the complexes are reported. $[Au_2(p\text{-tc})_2(dppb)]$ (**4**) crystallizes in the triclinic space group $P\bar{1}$ ($Z = 2$) with unit cell dimensions $a = 10.757(2)$ Å, $b = 13.177(2)$ Å, $c = 14.630(3)$ Å, $\alpha = 82.23(1)°$, $\beta = 83.16(1)°$, and $\gamma = 75.42(1)°$; $R = 0.0286$. $[Au_2(p\text{-tc})_2(dpppn)]$ (**5**) crystallizes in the monoclinic space group $P2_1/n$ ($Z = 4$) with unit cell dimensions $a = 12.007(1)$ Å, $b = 25.292(5)$ Å, $c = 13.421(2)$ Å, and $\beta = 94.92(1)°$; $R = 0.0432$. The structures of **4** and **5** are similar; each has linear, two-coordinate gold atoms connected via a bridging bis(phosphine) to form an open-chain dinuclear complex. The dinuclear units are then connected via short intermolecular gold(I)–gold(I) interactions to form polymeric chains. The intermolecular Au–Au distances for **4** and **5** are 3.094(1) and 3.200(1) Å, respectively. Other similar complexes include $[Au_2(p\text{-tc})_2(dppm)]$ (**1**), $[Au_2(p\text{-tc})_2(dppe)]$ (**2**), and $[Au_2(p\text{-tc})_2(dppp)]$ (**3**). Cyclic dinuclear gold(I) complexes with bridging bis(phosphine) and dithiolate ligands are also reported: [Au(dppe)(pdt)Au] (**6**), [Au(dppp)(pdt)Au] (**7**), [Au(dppb)(pdt)Au] (**8**), [Au(dpppn)(pdt)Au] (**9**), and [Au(dppe)(tdt)Au] (**10**). The following abbreviations are used: dppm = bis(diphenylphosphino)methane; dppe = 1,2-bis(diphenylphosphino)ethane; dppp = 1,3-bis(diphenylphosphino)propane; dppb = 1,4-bis(diphenylphosphino)butane; dpppn = 1,5-bis(diphenylphosphino)pentane; PMe_3 = trimethylphosphine; PPh_3 = triphenylphosphine; *p*-tc = *p*-thiocresol; pdt = 1,3-propanedithiol; tdt = 3,4-toluenedithiol. Spectral features of the dinuclear gold complexes are compared to those of the mononuclear complexes $Au(PPh_3)(p\text{-tc})$ (**11**) and $Au(PMe_3)(p\text{-tc})$ (**12**). Analysis of the electronic absorption spectra from Gaussian band spectral fitting, comparison to free ligand spectra, studies of solvatochromism, and alterations of the phosphine and thiolate ligands indicate that the two lowest energy transitions in **1–9**, **11**, and **12** are LMCT (S → Au) transitions. The spectra for the open-chain complexes, **2–5** in which the length of the bis(phosphine) backbone successively increases by 1, are very similar and show no absorption bands below 3.0×10^4 cm^{-1}. However, the lowest energy transition for the smallest member of this series, **1** (which is yellow), is significantly red shifted, occurring at 2.8×10^4 cm^{-1}. A similar trend is observed for the two smallest members of the cyclic series, **6** and **7** compared to **8** and **9**. Variable-temperature NMR experiments reveal the presence of dynamic processes for **1**, **6**, and **9**. The activation energy, determined by line shape analysis, is approximately 10 kcal/mol for **1** and **9** and less than 10 kcal/mol for **6**. The observed red shift in the LMCT transitions and the variable-temperature behavior are consistent with the presence of intramolecular gold(I)–gold(I) interactions in solution for **1** and **6–9**. The implications of these results for biological systems are considered.

Introduction

Gold(I) thiolate complexes have been used for the treatment of rheumatoid arthritis for over 60 years, despite the fact that the mechanism by which these drugs affect the course of the disease is not well understood.[2] Water-soluble, injectable gold drugs such as Myochrysine [gold(I) sodium thiomalate] and Solganol [gold(I) thioglucose] are anionic and exist as gold–thiolate oligomers in solution.[3] In contrast, the orally administered drug Auranofin [(tetraacetylthioglucose)(triethylphosphine)gold(I)], approved for use in the 1980s, is a neutral, mononuclear gold complex composed of phosphine as well as thiolate ligands.[4] In addition to the importance of thiolate ligands in the formulation of gold drugs, binding of gold(I) to thiolate functions in proteins is expected to play a key role in the molecular pharmacology of gold. For example, it is well established that gold circulates in the bloodstream bound to cysteine-34 in the protein albumin, and facile thiolate exchange reactions have been proposed to account for transport of gold from the bloodstream to joints and organs throughout the body.[5]

An intriguing phenomenon in gold chemistry which has received attention in both theoretical and experimental studies is the propensity for weak bonding interactions between closed shell,

* Corresponding authors. Comments concerning the crystal structure should be addressed to R.C.E.
† Upward Bound student.
‡ Project SEED student.

(1) (a) University of Maine. (b) University of Cincinnati. (c) Present address: Department of Chemistry, Princeton University, Princeton, NJ 08544.

(2) (a) Walz, D. T. Mechanisms of Action of Gold Salts in Rheumatoid Arthritis. In *Advances in Inflammation Research*; Otterness, I., Capetola, R., Wong, S., Eds.; Raven Press: New York, 1984; Vol. 7, p 239. (b) Brown, D. H.; Smith, W. E. *Chem. Soc. Rev.* **1980**, *9*, 217. (c) Shaw, C. F., III. *Inorg. Perspect. Biol. Med.* **1979**, *2*, 287. (d) Sadler, P. J. *Struct. Bonding (Berlin)* **1976**, *29*, 171.

(3) (a) Elder, R. C.; Ludwig, K.; Cooper, J. N.; Eidsness, M. K. *J. Am. Chem. Soc.* **1985**, *107*, 5024. (b) Al-Sa'ady, A. K. H.; Moss, K.; McAuliffe, C. A.; Parish, R. V. *J. Chem. Soc., Dalton Trans.* **1984**, 1609. (c) Isab, A. A.; Sadler, P. J. *J. Chem. Soc., Dalton Trans.* **1981**, 1657. (d) Isab, A. A.; Sadler, P. J. *J. Chem. Soc., Chem. Commun.* **1976**, 1051.

(4) (a) Sutton, B. M.; McGusty, E.; Walz, D. T.; DiMartino, M. J. *J. Med. Chem.* **1972**, *15*, 1095. (b) Hill, D. T.; Sutton, B. M. *Cryst. Struct. Commun.* **1980**, *9*, 679. (c) See ref 3a.

(5) (a) Shaw, C. F., III; Coffer, M. T.; Klingbeil, J.; Mirabelli, C. K. *J. Am. Chem. Soc.* **1988**, *110*, 729. (b) Coffer, M. T.; Shaw, C. F., III; Eidsness, M. K.; Watkins, J. W., II; Elder, R. C. *Inorg. Chem.* **1986**, *25*, 333. (c) Isab, A. A.; Sadler, P. J. *J. Chem. Soc., Dalton Trans.* **1982**, 135. (d) Snyder, R. M.; Mirabelli, C. K.; Crooke, S. T. *Biochem. Pharmacol.* **1986**, *35*, 923.

0020-1669/93/1332-2506$04.00/0

d^{10} gold(I) atoms.[6] In the solid state, evidence for a weak bond between gold atoms is provided by Au(I)–Au(I) separations (2.78–3.25 Å), which are less than the van der Waals radii for gold.[7] Schmidbaur et al. have estimated the strength of gold–gold interactions on the order of 5–15 kcal/mol.[6a] This estimate is based upon the observation that coordination of a bis(phosphine) molecule to two Au(I)–Cl fragments alters the ground-state conformation of the phosphine ligand as a result of a gold(I)–gold(I) interaction (eq 1).[8] The energies of gold(I)–gold(I) bonds

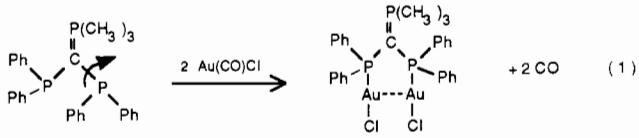

(1)

are the same order of magnitude as those of hydrogen bonds, which are important factors for determining protein structure and function. An interesting question to consider is whether gold–gold interactions can form under biological conditions and, if so, whether they can influence protein conformation and function.

We are investigating several series of neutral, dinuclear gold(I) complexes containing phosphine and thiolate ligands, in which the length of the bridging bis(phosphine) backbone is systematically changed (see Table I). In **1–5**, the number of methylene groups in the bis(phosphine) backbone increases from 1 to 5, forming an increasingly larger series of *open-chain*, dinuclear gold complexes. The same series of bis(phosphines) are used in **6–9**; however use of an aliphatic dithiolate is expected to create an increasingly larger series of *cyclic*, dinuclear gold complexes. Finally, by using an aromatic dithiolate, a more rigid, cyclic dinuclear gold complex should be formed (**10**). Our short-term goals are (1) to investigate the structure and bonding (in the solid state and solution) in these dinuclear gold complexes, with the specific aim of determining whether gold(I)–gold(I) interactions occur and (2) to determine if the occurrence of gold(I)–gold(I) interactions can be correlated with ring size (which is directly related to the number of methylene units in the bis(phosphine) backbone) or rigidity of the complex. Our longer term goals are to use the information obtained from studies on model complexes to investigate the occurrence of gold(I)–gold(I) interactions under more biologically relevant conditions.

Experimental Section

Reagents. All manipulations were performed under nitrogen, employing standard Schlenk and glovebox techniques.[9] Phosphines were obtained from Aldrich or Strem and used as received. $HAuCl_4 \cdot 3H_2O$, *p*-thiocresol ($CH_3C_6H_4SH$), 1,3-propanedithiol [$HS(CH_2)_3SH$], 3,4-toluenedithiol [$CH_3C_6H_3(SH)_2$], 3,4-dichlorobenzenethiol [$(Cl)_2C_6H_3SH$], and ethanolamine ($H_2NCH_2CH_2OH$) were purchased from Aldrich. Solvents were reagent grade and were used without further purification. Mononuclear and dinuclear gold phosphine chloride complexes were prepared as described in the literature.[10]

Instrumental Details. The NMR data were obtained on a Varian XL-200 FT-NMR spectrometer operating at 200 MHz for ^1H and 81 MHz for ^{31}P NMR. Phosphorus chemical shifts are referenced to external 85% H_3PO_4. Variable-temperature $^{31}P\{^1H\}$ NMR data were obtained for **1** (0.035 and 0.069 M), **4** (0.07 M), **6** (saturated solution), **9** (saturated solution), and **11** (0.05 M) in CD_2Cl_2 from +20 to −80 °C. Variable-temperature ^1H NMR data were obtained for **1** (0.02 M) in CD_2Cl_2 from +20 to −80 °C. Carbon and hydrogen elemental analyses were performed by Galbraith Laboratories, Knoxville, TN.

UV–Visible Spectra and Spectral Fits. Electronic absorption spectra were measured in 1.0-cm quartz cuvettes using a Hewlett Packard 8452 diode array spectrophotometer. Typically, four dilutions of each complex were prepared in the concentration range (0.12–1.9) x 10^{-4} M. No deviations from Beer's law behavior were observed for any complex. Spectra Calc (Galactic Industries) was used to manipulate, spectrally fit, and plot all electronic absorption spectra. The peak maxima and extinction coefficients were estimated for all clearly discernible peaks. The number and approximate positions of shoulders were estimated from the first derivative of the absorption spectra. Derivative spectra were examined at several concentrations to prevent including a false positive signal that may originate from noise in an absorption spectrum. The estimates of peak positions and extinction coefficients were used as input parameters for the spectral fitting program Curvefit (Spectra Calc) in which a set of Gaussian bands is iteratively fit to the experimental absorption spectrum. The spectral fit was considered complete when the change in χ^2 between successive iterations was small (<0.01% change/iteration) and the first derivative of the spectral fit closely matched the experimental derivative spectrum.

Abbreviations. The following abbreviations are used: dppm = bis(diphenylphosphino)methane; dppe = 1,2-bis(diphenylphosphino)-ethane; dppp = 1,3-bis(diphenylphosphino)propane; dppb = 1,4-bis(diphenylphosphino)butane; dpppn = 1,5-bis(diphenylphosphino)pentane; PMe_3 = trimethylphosphine; PPh_3 = triphenylphosphine; *p*-tc = *p*-thiocresol; pdt = 1,3-propanedithiol; tdt = 3,4-toluenedithiol.

General Synthesis. The gold(I) phosphine thiolate complexes listed in Table I were prepared by ligand substitution reactions of the corresponding gold(I) phosphine chloride complexes with alkane- or arenethiolates. The synthesis described below for **2** illustrates the general procedure.

$[Au_2(p\text{-tc})_2(dppe)]$ (2). An absolute ethanol solution of *p*-thiocresol (71.4 mg, 0.58 mmol) and ethanolamine (35 μL, 0.58 mmol) was slowly added to a solution of $[Au_2(Cl)_2(dppe)]$[10b] (250 mg, 0.29 mmol) in 15 mL of CH_2Cl_2. After 30 min of stirring, the solution volume was reduced and the flask was placed in an ice bath. The resulting pale yellow solid was filtered off and washed with ethanol (two times) and diethyl ether (two times). Yield: 85%. Repeated recrystallization from CH_2Cl_2/hexanes (or CH_2Cl_2/Et_2O) yields **2** as a white microcrystalline solid.

Yields of complexes **1–12**, before recrystallization, range from 50 to 90%. The yields are generally lower for the cyclic series (**6–9**) than for the open-chain series (**1–5**). Complexes **6–9** were recrystallized from warm $CHCl_3/Et_2O$. All complexes are white with the exception of **1**, which is bright yellow. Complex **1** is isolated as a sticky yellow solid; however repeated recrystallization from CH_2Cl_2/Et_2O or THF/pentane followed by drying in vacuo produces a yellow microcrystalline, hygroscopic solid. Elemental analyses and ^1H NMR spectra of two separate samples of **1** are consistent with the presence of 0.5 and 1.0 molecule of H_2O per molecule of **1**. Elemental analyses (C, H) and NMR data (^1H, ^{31}P) for **1–12** are provided below and in Table I, respectively. All complexes are soluble in CH_2Cl_2 or $CHCl_3$ and are slightly soluble in CH_3CN. The cyclic dinuclear gold complexes with the propanedithiol ligand (**6–9**) are in general less soluble than the open-chain dinuclear complexes (**1–5**), and the solubility decreases with increasing ring size. Complex **1** exhibits the greatest solubility in the solvents mentioned above and is also soluble in acetone and THF.

Elemental Analysis for 1–12. Calcd for **1**·H_2O ($C_{39}H_{36}Au_2P_2S_2 \cdot H_2O$): C, 44.92; H, 3.67. Found: C, 44.98; H, 3.83. Calcd for **2** ($C_{40}H_{38}Au_2P_2S_2$): C, 46.25; H, 3.69. Found: C, 46.19; H, 3.78. Calcd for **3** ($C_{41}H_{40}Au_2P_2S_2$): C, 46.78; H, 3.83. Found: C, 46.28; H, 3.76. Calcd for **4** ($C_{42}H_{42}Au_2P_2S_2$): C, 47.29; H, 3.97. Found: C, 47.03; H, 4.05. Calcd for **5** ($C_{43}H_{44}Au_2P_2S_2$): C, 47.78; H, 4.12. Found: C, 47.69; H, 4.25. Calcd for **6** ($C_{29}H_{30}Au_2P_2S_2$): C, 38.76; H, 3.37. Found: C, 38.29; H, 3.37. Calcd for **7** ($C_{30}H_{32}Au_2P_2S_2$): C, 39.48; H, 3.53. Found: C, 39.54; H, 3.61. Calcd for **8** ($C_{31}H_{34}Au_2P_2S_2$): C, 40.18; H, 3.70. Found: C, 39.88; H, 3.66. Calcd for **9** ($C_{32}H_{36}Au_2P_2S_2$): C, 40.86; H, 3.86. Found: C, 40.31; H, 3.85. Calcd for **10** ($C_{33}H_{30}Au_2P_2S_2$): C, 41.86; H, 3.35. Found: C, 41.82; H, 3.17. Calcd for **11** ($C_{25}H_{22}AuPS$): C, 51.55; H, 3.81. Found: C, 51.16; H, 3.91. Calcd for **12** ($C_{10}H_{16}AuPS$): C, 30.31; H, 4.07. Found: C, 30.22; H, 4.12.

X-ray Characterization of $[Au_2(p\text{-tc})_2(dppb)]$ (4) and $[Au_2(p\text{-tc})_2(dpppn)]$ (5). Crystals were formed by slow diffusion of ethyl ether into dichloromethane solutions at −10 °C. Colorless prisms were cut to

(6) (a) For a recent review see: Schmidbaur, H. *Gold Bull.* **1990**, *23*, 11. (b) Pyykkö, P.; Zhao, Y. *Angew. Chem., Int. Ed. Engl.* **1991**, *30*, 604. (c) Balch, A. L.; Fung, E. Y.; Olmstead, M. M. *J. Am. Chem. Soc.* **1990**, *112*, 5181. (d) Raptis, R. G.; Fackler, J. P., Jr.; Murray, H. H.; Porter, L. C. *Inorg. Chem.* **1989**, *28*, 4057. (e) King, C.; Wang, J.-C.; Khan, M. N. I.; Fackler, J. P., Jr. *Inorg. Chem.* **1989**, *28*, 2145. (f) Jiang, Y.; Alvarez, S.; Hoffmann, R. *Inorg. Chem.* **1985**, *24*, 749.
(7) Bondi, A. *J. Phys. Chem.* **1964**, *68*, 441.
(8) Schmidbaur, H.; Graf, W.; Müller, G. *Angew. Chem., Int. Ed. Engl.* **1988**, *27*, 417.
(9) Shriver, D. F.; Drezdon, M. A. *The Manipulation of Air-Sensitive Compounds*, 2nd ed.; Wiley: New York, 1986.
(10) (a) Mann, F. G.; Wells, A. F.; Purdie, D. *J. Chem. Soc.* **1937**, 1828. (b) Mirabelli, C.K.; Hill, D. T.; Faucette, L. F.; McCabe, F. L.; Girard, G. R.; Bryan, D. B.; Sutton, B. M.; Bartus, J. O.; Crooke, S. T.; Johnson, R. K. *J. Med. Chem.* **1987**, *30*, 2181.

Table I. NMR Data for **1–12**[a]

	compound	$^{31}P\{^1H\}$ NMR δ, ppm	$^{31}P\{^1H\}$ NMR Δ,[b] ppm	^1H NMR δ, ppm
1	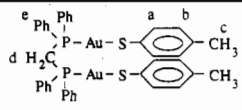	29.2	52.0	a+e: 7.28–7.73, m, 24H b: 6.86, d, *J*(HH) = 8 Hz, 4H c: 2.25, s, 6H d: 3.95, t, *J*(PH) = 10 Hz, 2H
2	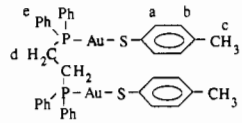	36.9	49.9	a+e: 7.34–7.81, m, 24H b: 6.92, d, *J*(HH) = 8 Hz, 4H c: 2.26, s, 6H d: 2.67, s, 4H
3	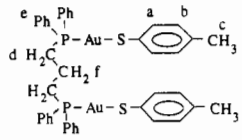	32.0	49.8	a+e: 7.29–7.81, m, 24H b: 6.89, d, *J*(HH) = 8 Hz, 4H c: 2.25, s, 6H d: 2.80, dt, *J*(PH) = 10 Hz, *J*(HH) = 7 Hz, 4H f: 1.93, m, 2H
4	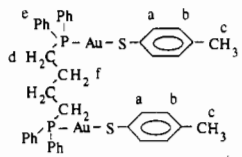	34.9	51.2	a+e: 7.33–7.79, m, 24H b: 6.57, d, *J*(HH) = 8 Hz, 4H c: 2.25, s, 6H d: 2.39, br, 4H f: 1.78, br, 4H
5	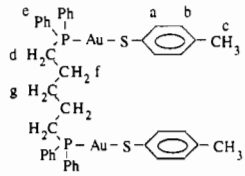	34.1	50.4	a+e: 7.35–7.85, m, 24H b: 6.88, d, *J*(HH) = 8 Hz, 4H c: 2.23, s, 6H d: 2.37, br, 4H f+g: 1.68, br, 6H
6	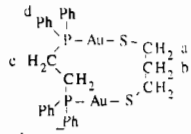	34.7	47.7	a: 3.63, t, *J*(HH) = 6 Hz, 4H b: 2.01, br, 2H c: 2.72, d, *J*(PH) = 13 Hz, 4H d: 7.33–7.94, m, 20H
7	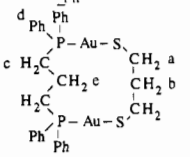	28.6	46.4	a: 3.45, t, *J*(HH) = 6 Hz, 4H b+e: 2.05, m, 4H c: 2.92, dt, *J*(PH) = 10 Hz, *J*(HH) = 7 Hz, 4H d: 7.36–7.94, m, 20H
8	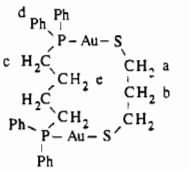	33.5	49.8	a: 3.36, t, *J*(HH) = 7 Hz, 4H b: 2.25, quin, *J*(HH) = 7 Hz, 2H c: 2.47, m, 4H d: 7.36–7.83, m, 20H e: 1.90, m, 4H
9	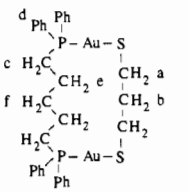	35.2	51.5	a: 3.26, t, *J*(HH) = 7 Hz, 4H b: 2.15, quin, *J*(HH) = 7 Hz, 2H c: 2.50, m, 4H d: 7.35–7.88, m, 20H e+f: 1.77, br, 6H
10	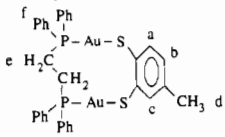	32.2	45.2	a+c+f: 7.15–7.90, m, 22H b: 6.76, d, *J*(HH) = 12 Hz, 1H d: 2.30, s, 3H e: 2.60, s, 4H
11	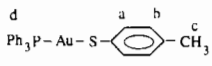	39.2	47.2	a+d: 7.39–7.69, m, 17H b: 6.93, d, *J*(HH) = 8 Hz, 2H c: 2.26, s, 3H
12	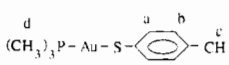	−1.7		a: 7.41, d, *J*(HH) = 8 Hz, 2H b: 6.91, d, *J*(HH) = 8 Hz, 2H c: 2.26, s, 3H d: 1.57, d, *J*(PH) = 11 Hz, 9H

[a] In chloroform. [b] Δ = coordination chemical shift = δ(complex) − δ(free ligand).[48]

the dimensions specified in Table II, mounted on glass fibers with epoxy cement, and transferred to a Siemens R3m/V four-circle diffractometer for characterization and data collection. Unit cell parameters (see Table II) were determined from the angular settings of 25 well-centered reflections: $24° < 2\theta < 31°$ for **4**; $23° < 2\theta < 32°$ for **5**. Axial photographs and a limited search through an octant of reciprocal space revealed a lack of systematic absences and symmetry consistent with the triclinic space group $P1$ or $P\bar{1}$ for **4** and the monclinic space group $P2_1/n$ for **5**. Complete

Table II. Crystal Data for $[Au_2(p\text{-tc})_2(dppb)]$ (**4**) and $[Au_2(p\text{-tc})_2(dpppn)]$ (**5**)

	4	**5**
chem formula	$C_{42}H_{42}Au_2P_2S_2$	$C_{43}H_{44}Au_2P_2S_2$
fw	1066.8	1080.9
crystal size, mm	0.08 × 0.12 × 0.25	0.14 × 0.25 × 0.28
space group	$P\bar{1}$ (No. 2)	$P2_1/n$ (No. 14)
crystal system	triclinic	monoclinic
a, Å	10.757(2)	12.007(1)
b, Å	13.177(2)	25.292(5)
c, Å	14.630(3)	13.421(2)
α, deg	82.23(1)	
β, deg	83.16(1)	94.92(1)
γ, deg	75.42(1)	
V, Å^3	1980.6(6)	4061(1)
Z	2	4
μ, cm^{-1}	75.86	73.98
D_c, g cm^{-3}	1.79	1.77
T, K	294	294
radiation (λ, Å)	Mo Kα (0.710 73)	Mo Kα (0.710 73)
extinction cor	0.000 36(2)	none
$R(F)$,[a] %	2.86	4.32
$R_w(F)$,[b] %	2.83	4.63
goodness of fit (S)[c]	1.14	1.35

[a] $R(F) = \sum(||F_o|-|F_c||)/\sum(|F_o|)$. [b] $R_w(F) = [\sum(w||F_o|-|F_c||^2)/\sum w|F_o|^2]^{1/2}$, where $w = [s^2(F) + |g|F^2]^{-1}$. [c] $S = [\sum(w||F_o| - |F_c||^2)/(M - N)]^{1/2}$.

details of the data collection are presented in Table II. The data were corrected for Lorentz–polarization and absorption effects (empirical correction based on five azimuthal reflections).

The structures were successfully solved by heavy-atom methods (XS: PATT) and refined by full-matrix least-squares procedures. The non-hydrogen atoms were refined with anisotropic temperature parameters, hydrogen atoms were allowed to ride on their respective carbons [C–H = 0.96 Å, U(H) = 0.08], and a weighting scheme based on $\sigma(F)$ was employed. Calculations were performed by using the SHELXTL PLUS package of programs.[11] Refinement converged to the R factors reported in Table II. The largest and mean |shift/esd| in the final cycles for both structures were 0.001 and 0.000, respectively. The minimum and maximum excursions in the final difference Fourier map for **4** were –0.64 and 1.06 e Å^{-3}, respectively. The final map contained two residual peaks corresponding to roughly 1 e Å^{-3}. These were situated 1.00 and 0.97 Å from Au(1) and Au(2) and are attributed to those atoms, respectively. The minimum and maximum excursions in the final difference Fourier map for **5** were –2.33 and 1.13 e Å^{-3}, respectively. The five largest residual peaks in the final difference map were all situated near the two gold atoms of the structure. All the remaining residuals were less than 1 e Å^{-3}.

(11) SHELXTL PLUS 3.43 for R3/V and R3m/V crystallographic systems: G. M. Sheldrick, University of Göttingen, Germany, and Siemens/Nicolet Analytical X-ray Instruments, Inc., Madison, WI, 1989. Neutral-atom scattering factors were used as stored in the SHELXTL PLUS structure determination package.

(12) (a) A reviewer raised the possibility of the formation of oligomers, especially for the cyclic series of complexes. Oligomers consisting of four or more gold atoms bridged by sulfur in open-chain or cyclic structures are unlikely for the following reasons: (1) formation of neutral oligomers in the *p*-tc series is unlikely given the Au:P:S ratios imposed by elemental analysis and ^{1}H NMR spectra; (2) neutral tetramers or hexamers are possible in the pdt series but would probably be very insoluble and would produce more complex ^{1}H and ^{31}P NMR spectra; (3) FAB mass spectra were obtained for **6** and **8** (suspended in *m*-nitrobenzyl alcohol) on a JEOL-SX mass spectrometer operating in the positive-ion mode. The complexity of the spectra are consistent with a significant amount of fragmentation and ion-molecule recombination, making interpretation of the spectra difficult. However in both cases the most intense peaks occur below m/z 1050 and a parent ion peak for **8** is observed at m/z 927 ($M + H^+$), consistent with a cyclic dinuclear structure. In addition, there are no peaks at the m/z ratios expected for tetramers (1793 for **6**; 1849 for **8**); and (4) Fackler et al. have recently prepared and structurally characterized the smallest member of the cyclic series, [Au(dppm)(pdt)Au], and the X-ray study reveals a cyclic dinuclear structure with a short intramolecular Au–Au contact.[12b] Finally, aggregation in solution as a result of intermolecular gold–gold bonds can also be ruled out on the basis of concentration-independent UV–visible spectra.[12c] (b) Dávila, R. M.; Elduque, A.; Grant, T.; Staples, R. J.; Fackler, J. P., Jr. *Inorg. Chem.*, submitted for publication. (c) Kawamura, T.; Ogawa, T.; Yamabe, T.; Masuda, H.; Taga, T. *Inorg. Chem.* **1987**, *26*, 3547.

Results and Discussion

Syntheses. The complexes listed in Table I are prepared by ligand substitution reactions of gold(I) phosphine chloride complexes with arene- or alkanethiolates (eqs 2–4). Thiols are

$$[Au_2Cl_2(Ph_2P(CH_2)_nPPh_2)] + 2[BH][SC_6H_4CH_3] \rightarrow [Au_2(SC_6H_4CH_3)_2(Ph_2P(CH_2)_nPPh_2)] + 2BHCl \quad (2)$$

$$n = 1\text{–}5,\ B = H_2NCH_2CH_2OH$$

$$[Au_2Cl_2(Ph_2P(CH_2)_nPPh_2)] + [BH]_2[S_2R] \rightarrow [Au(Ph_2P(CH_2)_nPPh_2)(S_2R)Au] + 2BHCl \quad (3)$$

$$n = 2\text{–}5,\ R = (CH_2)_3;\ n = 2,\ R = 3,4\text{-}C_6H_3CH_3$$

$$Au(PR'_3)Cl + [BH][SC_6H_4CH_3] \rightarrow Au(PR'_3)(SC_6H_4CH_3) + BHCl \quad (4)$$

$$R' = C_6H_5,\ CH_3$$

deprotonated with ethanolamine prior to reaction with the gold chloride complexes. The open-chain, dinuclear gold complexes **1–5** are prepared by reaction 2, and cyclic, dinuclear complexes **6–10** are obtained in reaction 3.[12] The mononuclear gold complexes **11** and **12** were prepared (eq 4) for purposes of spectral comparison to the dinuclear gold complexes. These reactions are fairly straightforward; however they do not proceed as expected for all phosphine and thiolate ligands. For example, the yield of **6** (eq 3; n = 2, R = $(CH_2)_3$) is decreased by a side reaction that forms $[Au(dppe)_2][Cl]$, which was characterized by comparison of its ^{1}H and ^{31}P NMR data to literature values.[13] In addition, small amounts of insoluble white solids (possibly gold–thiolate polymers) typically form in reaction 3 that are separated from the desired products during recrystallization.

Attempts to prepare larger ring analogues of **6–9**, i.e. by using butanedithiol in place of propanedithiol (pdt), result in the formation of highly insoluble white solids that are presumably polymeric in nature.[14] Another problem was encountered in attempts to extend the series of complexes containing toluenedithiol (tdt) to include longer chain phosphines (dppp, dppb, etc). In this case the major products isolated are green solids (possibly a result of oxidation of gold) that have not yet been completely characterized; only low yields of the desired white products (e.g. [Au(dppp)(tdt)Au]) are obtained. Attempts to prepare gold(I) complexes with monophosphine and dithiol ligands have also met with limited success. Reactions of propanedithiol (pdt) and R_3PAuCl (R = Me, Et, Ph) generally result in very low yields of the desired products or produce insoluble solids, while reactions of tdt and R_3PAuCl result in mixtures of white and green solids.[15]

Complexes **2–12** are typically isolated as pale yellow or off-white solids. However, repeated recrystallization yields analytically pure, white complexes. Interestingly, **1** is bright yellow, a color which is atypical for linear, two-coordinate Au(I) complexes. The unusual color of **1** prompted us to investigate whether oxidative addition of CH_2Cl_2 (solvent) had occurred. To rule out this possibility, **1** was prepared in acetone solution and

(13) (a) Berners-Price, S. J.; Sadler, P. J. *Inorg. Chem.* **1986**, *25*, 3822. (b) Berners-Price, S. J.; Mazid, M. A.; Sadler, P. J. *J. Chem. Soc., Dalton Trans.* **1984**, 969.

(14) An earlier recorded attempt to prepare a gold(I) complex with bridging bis(phosphine) and dithiolate ligands also led to the formation of insoluble polymers: Weinstock, J.; Sutton, B. M.; Kuo, G. Y.; Walz, D. T.; Martino, M. J. *J. Med. Chem.* **1974**, *17*, 137.

(15) One of the products from the reaction of Et_3PAuCl and tdt has been characterized by FAB-MS, elemental analysis, and a preliminary X-ray study as an unusual tetragold complex, $Au_4(tdt)_2(PEt_3)_2$: Narayanaswamy, R.; Ho, D. M.; Bruce, A. E.; Bruce, M. R. M. Unpublished results. The crystal structure of this complex has recently been solved by Fackler, J. P., Jr., et al.[12b]

Table III. Fractional Atomic Positional Parameters for Non-Hydrogen Atoms ($\times 10^4$) and Equivalent Isotropic Displacement Parameters ($Å^2 \times 10^3$) for **4**

atom	*x*	*y*	*z*	*U*(eq)
Au(1)	3568(1)	−1256(1)	2936(1)	42(1)
Au(2)	2540(1)	1158(1)	2530(1)	44(1)
S(1)	1708(1)	−915(1)	3916(1)	63(1)
S(2)	1326(2)	494(1)	1670(1)	62(1)
P(1)	5462(1)	−1643(1)	2053(1)	37(1)
P(2)	3804(1)	1920(1)	3209(1)	40(1)
C(1)	5771(5)	−628(4)	1142(3)	43(2)
C(2)	4884(5)	−429(4)	367(4)	47(2)
C(3)	4318(5)	1378(4)	4352(4)	47(2)
C(4)	4828(6)	181(4)	4507(3)	49(2)
C(11)	5697(5)	−2828(4)	1489(3)	39(2)
C(12)	6786(6)	−3140(4)	875(4)	55(2)
C(13)	6996(7)	−4067(5)	481(5)	68(3)
C(14)	6137(8)	−4688(5)	683(5)	72(3)
C(15)	5057(8)	−4394(5)	1278(5)	72(3)
C(16)	4827(6)	−3454(5)	1683(4)	57(2)
C(21)	6807(5)	−1953(4)	2772(4)	44(2)
C(22)	7619(6)	−1276(5)	2747(5)	64(3)
C(23)	8607(6)	−1546(7)	3353(6)	86(4)
C(24)	8753(7)	−2439(8)	3965(6)	87(4)
C(25)	7937(8)	−3077(7)	3987(5)	83(3)
C(26)	6964(6)	−2849(5)	3395(4)	59(2)
C(31)	3067(5)	3282(4)	3379(4)	46(2)
C(32)	3805(7)	3985(5)	3436(5)	68(3)
C(33)	3247(8)	4995(5)	3639(5)	81(3)
C(34)	1942(8)	5330(5)	3781(5)	75(3)
C(35)	1190(7)	4657(6)	3718(5)	78(3)
C(36)	1738(6)	3630(5)	3515(4)	60(3)
C(41)	5230(5)	1966(4)	2425(4)	40(2)
C(42)	6495(5)	1594(5)	2665(4)	54(2)
C(43)	7514(6)	1595(5)	2000(5)	65(3)
C(44)	7303(7)	1989(5)	1097(5)	68(3)
C(45)	6069(6)	2385(5)	846(4)	58(3)
C(46)	5038(6)	2366(4)	1513(4)	49(2)
C(51)	1912(5)	−1870(4)	4888(4)	44(2)
C(52)	2894(6)	−2782(4)	4940(4)	51(2)
C(53)	2929(6)	−3534(5)	5714(5)	65(3)
C(54)	2016(7)	−3391(5)	6452(4)	61(3)
C(55)	1055(6)	−2474(5)	6411(5)	62(3)
C(56)	990(5)	−1736(5)	5646(4)	55(2)
C(57)	2082(8)	−4200(6)	7302(5)	92(4)
C(61)	842(5)	1483(5)	762(4)	49(2)
C(62)	495(5)	2561(5)	849(4)	52(2)
C(63)	−17(6)	3296(6)	150(5)	69(3)
C(64)	−218(7)	2985(8)	−685(5)	82(3)
C(65)	123(7)	1950(7)	−773(5)	76(3)
C(66)	644(6)	1196(6)	−89(5)	65(3)
C(67)	−757(9)	3781(8)	−1467(6)	131(5)

recrystallized several times from THF/pentane. This procedure yields analytically pure material of **1** which is still bright yellow. An explanation for the unusual color will be presented in the UV–visible studies.

Solid-State Structure of [Au_2(*p*-tc)$_2$(dppb)] (4). Crystal data and non-hydrogen atom coordinates for **4** are listed in Tables II and III, respectively, while selected bond distances and angles are given in Table IV. Two crystallographically independent molecules of **4** are present in the solid state, and these are shown in Figure 1A (molecules **4a** and **4b**). Molecules **4a** and **4b** possess open-chain structures with Au(*p*-tc) groups at each end of the chain and a bridging bis(phosphine) ligand in the middle. Each gold atom is two-coordinate and linearly bound to the sulfur of a *p*-tc thiolato anion and one of the phosphorus atoms of the bridging dppb ligand. The gold atoms are bound to the dppb ligand on opposite sides of the plane defined by the four carbon atoms of the chain. Both **4a** and **4b** possess crystallographic inversion symmetry (midpoint of the four-carbon chain) in the solid state. The presence of two conformationally different open-chain trans rotamers in the solid state is attributed to crystal packing and intermolecular forces (vide infra).

The most interesting feature in the structure of **4** is the presence of a short intermolecular Au(1)–Au(2) distance of 3.094(1) Å, which is significantly less than the van der Waals contact radii

Table IV. Selected Bond Distances (Å) and Angles (deg) in [Au_2(*p*-tc)$_2$(dppb)] (**4**)

Au(1)–Au(2)	3.094(1)	P(1)–C(1)	1.820(5)
Au(1)–S(1)	2.301(2)	P(1)–C(11)	1.812(6)
Au(1)–P(1)	2.260(1)	P(1)–C(21)	1.821(6)
Au(2)–S(2)	2.307(2)	P(2)–C(3)	1.820(6)
Au(2)–P(2)	2.263(2)	P(2)–C(31)	1.809(5)
S(1)–C(51)	1.762(5)	P(2)–C(41)	1.811(5)
S(2)–C(61)	1.758(6)		
Au(2)–Au(1)–S(1)	77.0(1)	Au(1)–P(1)–C(1)	116.6(2)
Au(2)–Au(1)–P(1)	105.1(1)	Au(1)–P(1)–C(11)	113.5(2)
S(1)–Au(1)–P(1)	176.4(1)	C(1)–P(1)–C(11)	105.7(2)
Au(1)–Au(2)–S(2)	77.0(1)	Au(1)–P(1)–C(21)	110.3(2)
Au(1)–Au(2)–P(2)	106.8(1)	C(1)–P(1)–C(21)	106.5(3)
S(2)–Au(2)–P(2)	172.9(1)	C(11)–P(1)–C(21)	103.1(2)
Au(1)–S(1)–C(51)	107.7(2)	Au(2)–P(2)–C(3)	120.0(2)
Au(2)–S(2)–C(61)	106.0(2)	Au(2)–P(2)–C(31)	113.1(2)

(3.4 Å)[7] and is indicative of a weak bonding interaction.[6] A consequence of this weak interaction is the further oligomerization of the open-chain digold **4a** and **4b** molecules into extended polymers via gold–gold bonds. A view of the extended chain is given in Figure 1B. The Au(1)–S(2) and Au(2)–S(1) distances are both 3.42 Å, indicating that the gold–gold bonds are not supported by bridging thiolate interactions.

The Au–P [2.260(1) and 2.263(2) Å] and Au–S [2.307(2) and 2.301(1) Å] distances in **4a** and **4b** are typical of two-coordinate gold(I) compounds,[16] as are the P–Au–S angles of 176.4(1) and 172.9° for **4a** and **4b**, respectively. Slight deviations from linearity are common for gold(I) structures, both with and without Au–Au contacts.[6a,17] The Au–P–C angles range from 110.3 to 116.6° [mean 113.5°] for **4a** and 108.0 to 120.0° [mean 113.7°] for **4b**, while the C–P–C angles range from 103.1 to 106.5° [mean 105.1°] for **4a** and 101.8 to 108.1° [mean 104.9°] for **4b**. All other bond lengths and angles are within the ranges normally observed.

Solid-State Structure of [Au_2(*p*-tc)$_2$(dpppn)] (5). Crystal data and atomic coordinates for **5** are listed in Tables II and V, respectively. Selected bond distances and angles are listed in Table VI. A view of **5** with atom labels is shown in Figure 2A. As with the previously described molecule **4**, complex **5** also possesses an open-chain structure with Au(*p*-tc) groups at each end of the chain. Again, the phosphorus–carbon–phosphorus chain is in the expected all-trans conformation and the gold atoms are on the opposite sides of the plane defined by the chain. There is no crystallographically required symmetry in molecules of **5**; however, there is an approximate 2-fold axis passing through C(3) and perpendicular to the plane of the figure.

There is also a gold–gold bond in **5**, as indicated by the somewhat longer distance of 3.200(1) Å versus 3.094(1) Å for **4**. That feature is shown in Figure 2B. The Au–P [2.265(3) and 2.272(2) Å] and Au–S [2.313(3) and 2.310(3) Å] distances are essentially as found in **4**. Again, there are slight deviations from linearity at gold. The Au(1)–S(2) and Au(2)–S(1) distances are 3.94 and 3.76 Å, respectively, excluding the possibility of any additional bridging thiolate interactions being present.

Solid-State Structures. The pairing of gold atoms either intra- or intermolecularly and the formation of polymers via metal–metal interactions are well-established phenomena in gold coordination chemistry.[6a,18] Several complexes which contain the linear fragment P–Au–Cl or P–Au–SR and exhibit intramolecular or intermolecular Au–Au interactions in the solid state are presented in Table VII. *Intramolecular* gold–gold contacts

(16) Colacio, E.; Romerosa, A.; Ruiz, J.; Román, P.; Gutiérrez-Zorrilla, J. M.; Vegas, A.; Martínez-Ripoll, M. *Inorg. Chem.* **1991**, *30*, 3743 and references therein.
(17) For example, in the structure of Auranofin, which has no gold–gold interaction, the S–Au–P angle is 173.6°.[4b]
(18) Perreault, D.; Drouin, M.; Michel, A.; Harvey, P. D. *Inorg. Chem.* **1991**, *30*, 2.
(19) Schmidbaur, H.; Wohlleben, A.; Wagner, F.; Orama, O.; Huttner, G. *Chem. Ber.* **1977**, *110*, 1748.

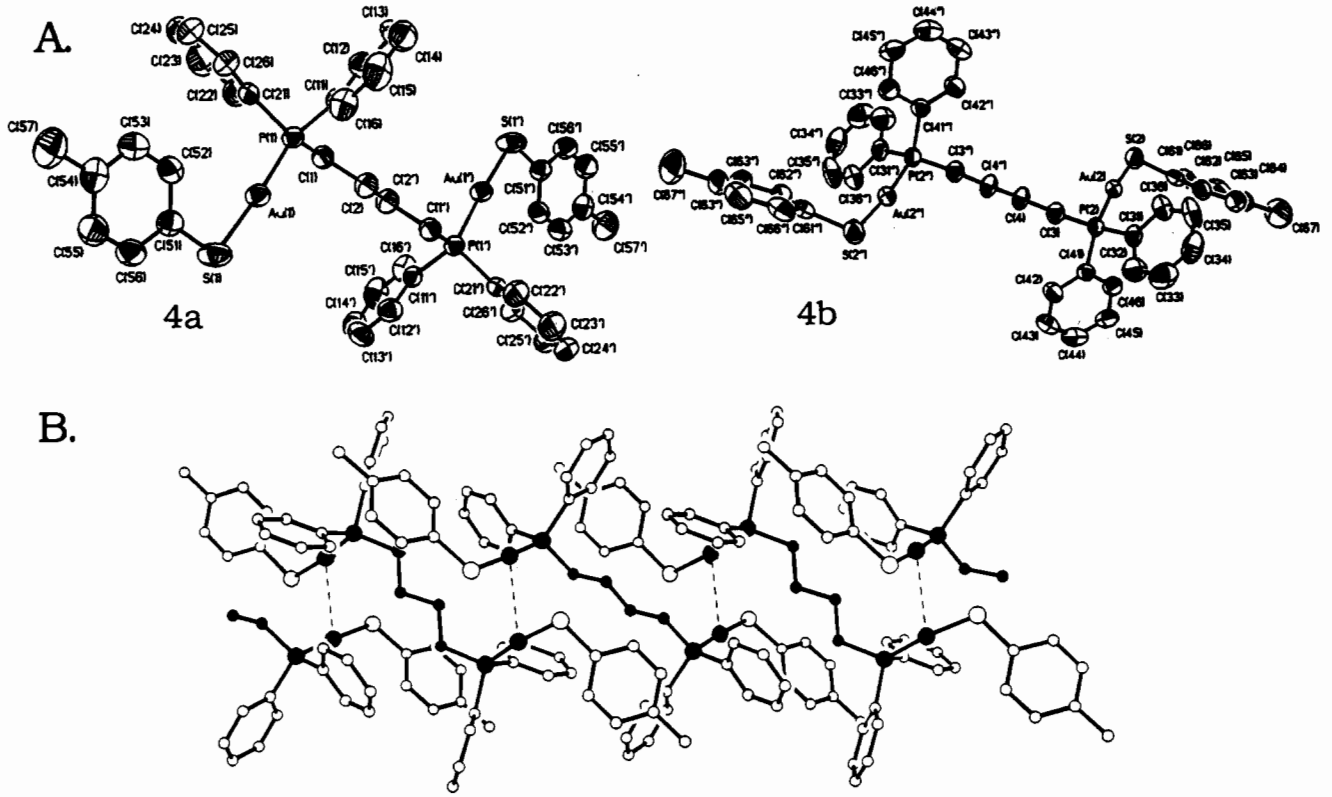

Figure 1. Structural views of $[Au_2(p\text{-tc})_2(dppb)]$ (**4**). (A) Atom-labeling scheme with 50% probability ellipsoids. Symmetry codes: $' = 1 - x, -y, -z$; $'' = 1 - x, -y, 1 - z$. (B) The polymeric structure in the lattice with gold(I)–gold(I) interactions shown as dashed lines. Au, P, and C (backbone) atoms are shaded.

have been demonstrated for three types of complexes: (i) those containing one or two carbon atoms connecting two phosphorus atoms in a bis(phosphine) ligand (entries 1–3), (ii) those containing two connecting carbons with restricted rotation about the C–C bond (entry 4), and (iii) cyclic complexes containing two bidentate bridging ligands (entry 5). *Intermolecular* gold–gold contacts have been observed (i) between pairs of sterically unhindered mononuclear gold complexes (entry 6), (ii) between pairs of open-chain dinuclear gold complexes (entries 7–10), and (iii) within extended polymers (entries 11–15).

To our knowledge, **4** and **5** (entries 14 and 15) represent unique examples of thiolate-containing gold phosphine complexes that form polymeric chains linked by intermolecular gold–gold bonds. Nevertheless it is interesting to note that in the 10-membered-ring complex $[Au_2(SCH_2CH_2PEt_2)_2]$ (entry 5), which contains an intramolecular Au–Au interaction, the Au–P (2.27 Å), Au–S (2.31Å), and Au–Au (3.104 Å) bond distances and the P–Au–S angle (173.5°)[22] are very similar to those found in **4** and **5** (see Tables IV and VI). Structures **4** and **5** can also be compared to the series of closely related open-chain gold chloride complexes shown in Table VII. Entries 1, 7 (or 8), and 13 represent gold chloride complexes in which the number of methylene groups in the bis(phosphine) alkyl backbone successively increases by 1. For entry 1, $[Au_2(Cl)_2(dppm)]$, there is an intramolecular Au–Au interaction at 3.351 Å. For entry 7 (or 8), $[Au_2(Cl)_2(dppe)]$, the extra methylene group significantly increases the intramolecular separation between gold atoms to ≈6.3 Å.[24] However, a shorter intermolecular gold–gold contact results (≈3.2 Å) through the formation of dimers, i.e. $[Au_2(Cl)_2(dppe)]_2$. Increasing the number of methylene groups to 3, entry 13, $[Au_2(Cl)_2(dppp)]$, results in the formation of infinite chains with a gold–gold interaction at 3.3 Å. Finally, complexes **4** and **5**, with four and five connecting methylene groups, respectively, also form polymeric structures which are very similar to entry 13.

Comparison of entries 1, 7, and 12–15 suggests that there may be a correlation between the bis(phosphine) backbone length and the nature of the gold–gold interaction in the solid state. However inspection of Table VII shows that length alone is not a good predictor of whether intramolecular or intermolecular gold–gold interactions form and whether the intermolecular interactions occur by formation of dimers or polymers. For example, both intramolecular and intermolecular interactions are observed from complexes with two connecting carbons in the bis(phosphine) backbone (compare entries 3 and 7). Also entry 10, which has a sterically bulky (Ph)As group as one of the three connecting groups in the bis(phosphine), is a dimer, while entries 12 and 13 with three connecting carbons are polymers. It is also apparent from this series of complexes that there is no correlation between the length of the bis(phosphine) backbone and the Au–Au distance. Finally, neither is there a correlation between the nature of the gold–gold interaction, i.e. intramolecular vs. intermolecular, and the Au–Au distance.

Electronic Absorption Spectra. Figures 3 and 4 present spectra for **5** and **1** in the absorbance (i) and derivative (ii) modes along with the results of spectral fits (iii and iv). The electronic absorption spectra for **1**–**12** consist of intense absorbances above 40 000 cm^{-1} (<250 nm) followed by a series of poorly defined shoulders at lower energy (e.g. Figure 3i). Subtle differences between complexes are more apparent in the derivative spectra since shoulders in an absorption spectrum correspond to inflection

(20) Dziwok, K.; Lachmann, J.; Wilkinson, D. L.; Müller, G.; Schmidbaur, H. *Chem. Ber.* **1990**, *123*, 423.
(21) Jones, P. G. *Acta Crystallogr.* **1980**, *B36*, 2775.
(22) Crane, W. S.; Beall, H. *Inorg. Chim. Acta* **1978**, *31*, L469.
(23) Schmidbaur, H.; Weidenhiller, G.; Steigelmann, O.; Müller, G. *Chem. Ber.* **1990**, *123*, 285.
(24) Bates, P. A.; Waters, J. M. *Inorg. Chim. Acta* **1985**, *98*, 125.
(25) Eggleston, D. S.; Chodosh, D. F.; Girard, G. R.; Hill, D. T. *Inorg. Chim. Acta* **1985**, *108*, 221.
(26) Ni Dhubhghaill, O. M.; Sadler, P. J.; Kuroda, R. *J. Chem. Soc., Dalton Trans.* **1990**, 2913.
(27) Eggleston, D. S.; McArdle, J. V.; Zuber, G. E. *J. Chem. Soc., Dalton Trans.* **1987**, 677.
(28) Schmidbaur, H.; Paschalidis, C.; Steigelmann, O.; Muller, G. *Chem. Ber.* **1989**, *122*, 1851.
(29) Cooper, M. K.; Mitchell, L. E.; Henrick, K.; McPartlin, M.; Scott, A. *Inorg. Chim. Acta* **1984**, *84*, L9.

Table V. Fractional Atomic Positional Parameters for Non-Hydrogen Atoms (×10⁴) and Equivalent Isotropic Displacement Parameters (Å² × 10³) for **5**

atom	x	y	z	U(eq)
Au(1)	4805(1)	2423(1)	1086(1)	39(1)
Au(2)	2229(1)	2231(1)	1420(2)	39(1)
S(1)	4574(2)	3206(1)	1935(2)	49(1)
S(2)	2761(3)	1699(1)	2776(2)	68(1)
P(1)	5224(2)	1692(1)	218(2)	38(1)
P(2)	1564(2)	2712(1)	68(2)	36(1)
C(1)	6355(7)	1820(4)	-572(7)	44(3)
C(2)	7408(7)	2007(5)	23(8)	58(4)
C(3)	8382(7)	2083(4)	-610(7)	49(4)
C(4)	9391(7)	2320(4)	-2(7)	54(4)
C(5)	10378(7)	2398(4)	-628(7)	45(3)
C(11)	4096(7)	1412(4)	-594(7)	38(3)
C(12)	3121(7)	1275(4)	-166(8)	46(3)
C(13)	2215(8)	1063(5)	-747(10)	68(5)
C(14)	2284(10)	995(5)	-1750(10)	73(5)
C(15)	3221(11)	1121(4)	-2184(9)	69(5)
C(16)	4149(8)	1328(4)	-1599(7)	55(4)
C(21)	5764(7)	1149(3)	1006(7)	40(3)
C(22)	6180(9)	1245(4)	1974(7)	54(4)
C(23)	6654(10)	839(5)	2554(9)	74(5)
C(24)	6701(10)	346(5)	2178(9)	80(5)
C(25)	6286(10)	241(4)	1218(9)	74(5)
C(26)	5818(8)	641(4)	631(8)	56(4)
C(31)	2559(7)	2822(4)	-856(6)	39(3)
C(32)	3363(8)	3212(5)	-702(7)	57(4)
C(33)	4219(8)	3266(5)	-1331(8)	72(5)
C(34)	4232(9)	2937(5)	-2138(8)	72(5)
C(35)	3398(9)	2563(5)	-2340(9)	66(5)
C(36)	2574(8)	2501(4)	-1692(7)	48(4)
C(41)	1087(7)	3363(4)	390(7)	44(3)
C(42)	322(9)	3644(4)	-228(9)	64(4)
C(43)	-34(10)	4129(5)	39(11)	77(5)
C(44)	397(11)	4354(5)	931(12)	88(6)
C(45)	1176(12)	4088(5)	1538(12)	91(6)
C(46)	1494(9)	3589(5)	1267(9)	66(5)
C(51)	5300(7)	3699(4)	1293(7)	40(3)
C(52)	5029(8)	4219(4)	1428(7)	48(4)
C(53)	5621(9)	4617(4)	1005(8)	59(4)
C(54)	6475(8)	4507(5)	391(8)	57(4)
C(55)	6722(8)	3977(5)	256(7)	56(4)
C(56)	6158(8)	3578(4)	674(7)	54(4)
C(57)	7121(9)	4942(5)	-50(10)	81(5)
C(61)	2361(10)	1061(4)	2316(8)	58(4)
C(62)	3150(10)	676(5)	2162(9)	69(5)
C(63)	2851(13)	193(5)	1777(10)	86(6)
C(64)	1721(14)	57(5)	1513(10)	85(6)
C(65)	934(11)	433(6)	1687(10)	85(6)
C(66)	1239(11)	925(5)	2078(10)	79(5)
C(67)	1438(14)	-465(6)	1022(11)	121(8)

Table VI. Selected Bond Distances (Å) and Angles (deg) in $[Au_2(p\text{-tc})_2(dpppn)]$ (**5**)[a]

Au(1)–Au(2)	3.200(1)	P(1)–C(1)	1.823(9)
Au(1)–S(1)	2.313(3)	P(1)–C(11)	1.808(8)
Au(1)–P(1)	2.265(3)	P(1)–C(21)	1.818(9)
Au(2)–S(2)	2.310(3)	P(2)–C(5″)	1.819(9)
Au(2)–P(2)	2.272(2)	P(2)–C(31)	1.815(9)
S(1)–C(51)	1.785(9)	P(2)–C(41)	1.808(10)
S(2)–C(61)	1.779(11)		
Au(2)–Au(1)–S(1)	84.4(1)	Au(1)–P(1)–C(1)	111.3(3)
Au(2)–Au(1)–P(1)	102.0(1)	Au(1)–P(1)–C(11)	116.2(3)
S(1)–Au(1)–P(1)	173.5(1)	C(1)–P(1)–C(11)	106.0(4)
Au(1)–Au(2)–S(2)	89.6(1)	Au(1)–P(1)–C(21)	113.6(3)
Au(1)–Au(2)–P(2)	94.9(1)	C(1)–P(1)–C(21)	103.1(4)
S(2)–Au(2)–P(2)	174.9(1)	C(11)–P(1)–C(21)	105.5(4)
Au(1)–S(1)–C(51)	106.0(3)	Au(2)–P(2)–C(5″)	112.5(3)
Au(2)–S(2)–C(61)	101.9(4)	Au(2)–P(2)–C(31)	114.9(3)

[a] Symmetry code: ″ = −1 + *x*, *y*, *z*.

points in the derivative mode (e.g., compare Figures 3ii and 4ii). Therefore the number and position of electronic transitions were estimated from the derivative spectra, and this information was used to set initial input parameters for the Gaussian band, spectral fitting procedure described in the Experimental Section. Spectral

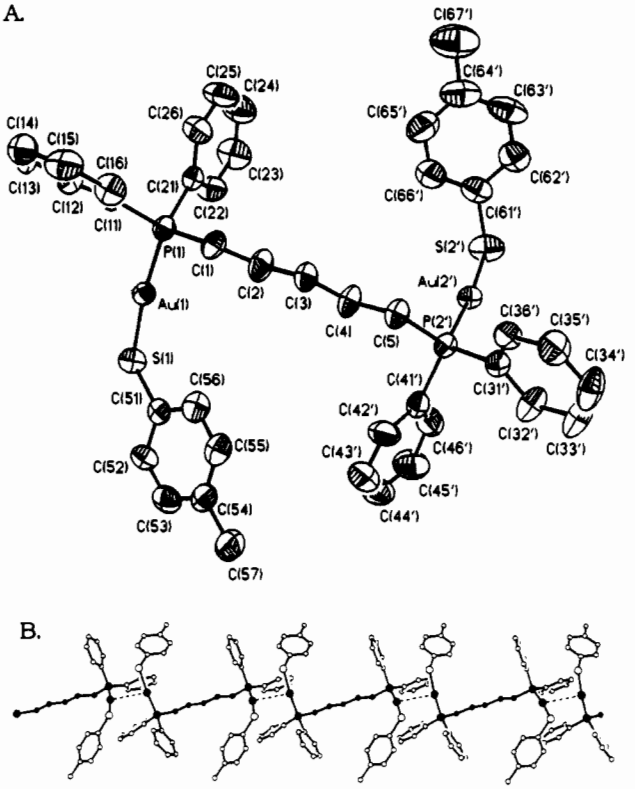

Figure 2. Structural views of $[Au_2(p\text{-tc})_2(dpppn)]$ (**5**). (A) Atom-labeling scheme with 50% probability ellipsoids. Symmetry code: ′ = 1 − *x*, *y*, *z*. (B) The polymeric structure in the lattice with gold(I)–gold(I) interactions shown as dashed lines. Au, P, and C (backbone) atoms are shaded.

Table VII. Comparison of Au–Au Interactions and Distances[a] for Structures Containing P–Au–L (L = Cl and SR)

entry	complex	Au–Au, Å	ref
	Intramolecular Au–Au Interactions		
1	$[Au_2(Cl)_2(dppm)]$	3.351(2)	19
2	$[Au_2(Cl)_2\{$(bis(diphenylphosphino)-methylene)trimethylphosphorane$\}]$	3.000(1)	8
3	$[Au_2(Cl)_2\{$1,1′-bis(diphenyl-phosphino)bicyclopropyl$\}]$	3.085(1)	20
4	$[Au_2(Cl)_2\{$*cis*-1,2-bis(diphenyl-phosphino)ethylene$\}]$	3.05(1)	21
5	$[Au_2(SCH_2CH_2PEt_2)_2]$	3.104	22
	Intermolecular Au–Au Interactions		
	Dimers		
6	$[Au(Cl)\{2,4,6\text{-}(Bu^t)_3C_6H_2PH_2\}]_2$	3.440(1)	23
7	$[Au_2(Cl)_2(dppe)]_2$	3.189(1)	24
8	$[Au_2(Cl)_2(dppe)]_2$	3.187(1), 3.221(1)	25
9	$[Au_2(Cl)_2\{Ph_2P(CH_2)_2AsPh_2\}]_2$	3.21	26
10	$[Au_2(Cl)_2\{Ph_2PCH_2As(Ph)\text{-}CH_2PPh_2\}]_2$	3.141(1)	6c
	Polymers		
11	$[Au_2(Cl)_2(\{$*trans*-1,2-bis(diphenyl-phosphino)ethylene$\}]_n$	3.043(1)	27
12	$[Au_2(Cl)_2\{Ph_2PCH_2C(CH_2)\text{-}CH_2PPh_2\}]_n$	3.294	28
13	$[Au_2(Cl)_2(dppp)]_n$	3.316	29
14	$[Au_2(p\text{-tc})_2(dppb)]_n$ (**4**)	3.094(1)	*b*
15	$[Au_2(p\text{-tc})_2(dpppn)]_n$ (**5**)	3.200(1)	*b*

[a] Estimated standard deviations in parentheses where available. [b] This work.

fits were also carried out for the dinuclear gold complexes **6** and **8** (Figures A and B, supplementary material). The remaining complexes were not spectrally fit because the absorption spectra for **2**–**4** are very similar to that for **5**, that for **7** is similar to that for **6**, and that for **9** is similar to that for **8**. To aid in assignments, spectral fits were also carried out for PPh_3, *p*-tc, $Au(PPh_3)(Cl)$, $Au(PPh_2Et)(Cl)$, **11**, and **12**. (The spectral fit for **11** is available as Figure C, suppplementary material.) The final values for

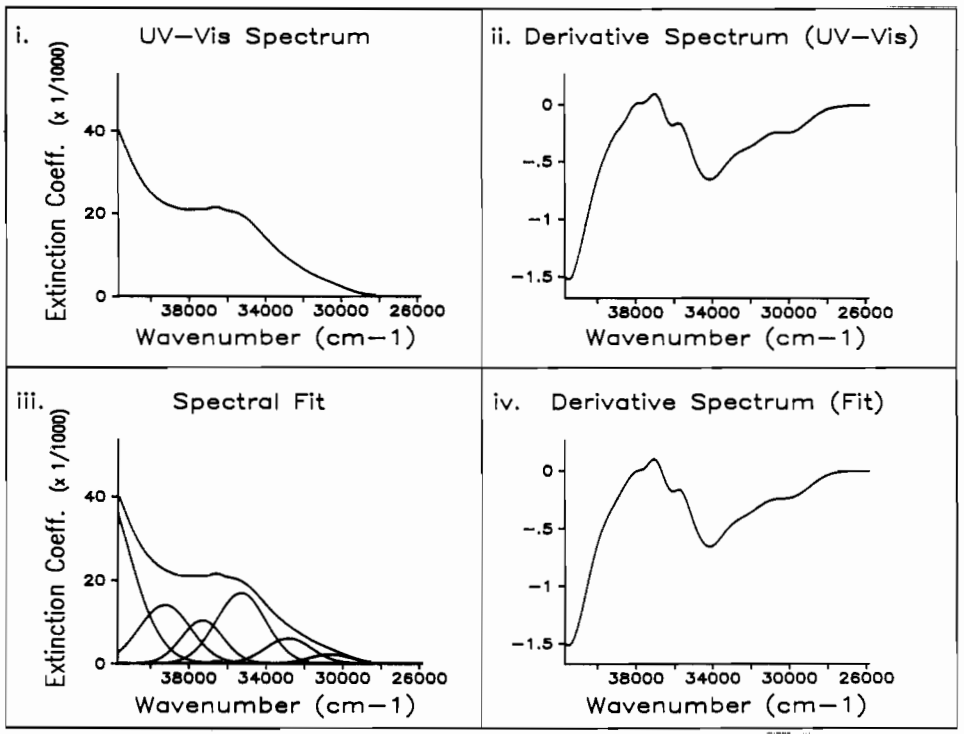

Figure 3. UV–visible absorption and derivative spectra for $[Au_2(p\text{-tc})_2(dpppn)]$ (**5**) in CH_2Cl_2: (i) experimental absorption spectrum; (ii) experimental derivative spectrum; (iii) spectral fit for absorption spectrum; (iv) spectral fit for derivative spectrum.

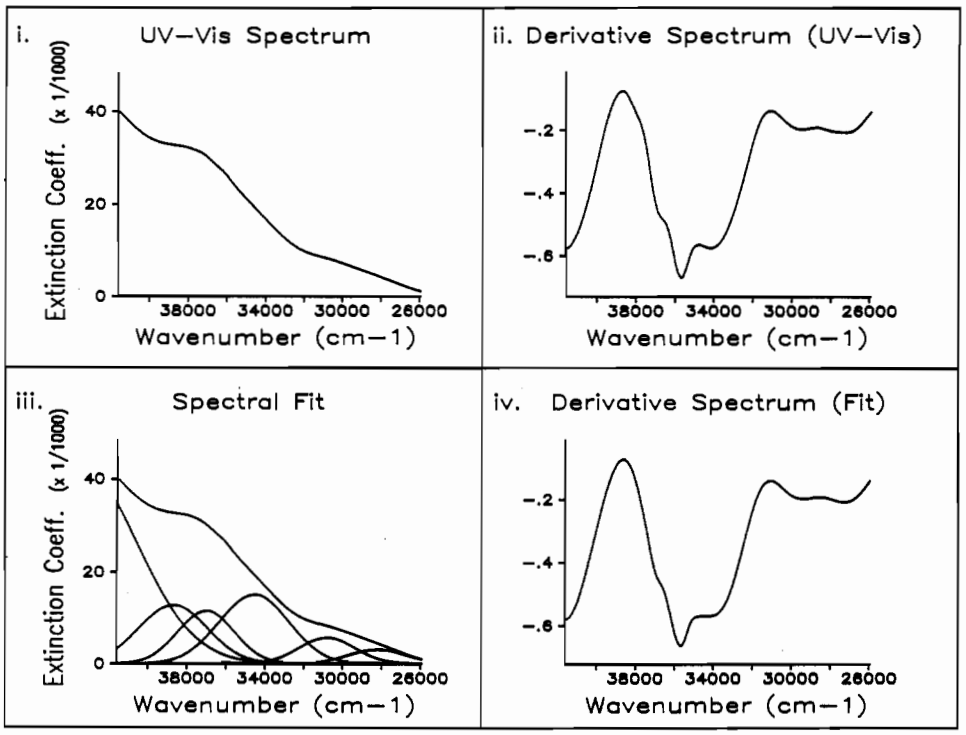

Figure 4. UV–visible absorption and derivative spectra for $[Au_2(p\text{-tc})_2(dppm)]$ (**1**) in CH_2Cl_2: (i) experimental absorption spectrum; (ii) experimental derivative spectrum; (iii) spectral fit for absorption spectrum; (iv) spectral fit for derivative spectrum.

peak positions and extinction coefficients obtained from spectral fits are summarized in Table VIII; in general, only absorbances below 3.9×10^4 cm^{-1} are included.[30] The assignments in Table VIII are based primarily upon comparisons to free-ligand spectra, studies of solvatochromism, and alterations of the phosphine and thiolate ligands. Previous assignments for related gold(I) complexes are also useful.

The two lowest energy absorbances in PPh_3, at 3.5×10^4 and 3.8×10^4 cm^{-1} have been assigned as $\pi \rightarrow \pi^*$ and $n \rightarrow \pi^*$ transitions, respectively.[31] The same assignments are reasonable for the two lowest energy bands in $Au(PPh_3)(Cl)$ and $Au(PPh_2Et)(Cl)$ since there is a close match in energy and intensity for these transitions upon coordination of PR_3.[32] The two lowest energy bands for *p*-tc at 3.5×10^4 and 3.6×10^4 cm^{-1} are also assigned as intraligand transitions in analogy to PPh_3.

In the spectrum of $Au(PMe_3)(p\text{-tc})$ (**12**), there are four bands

(30) All electronic transition maxima are reported to the nearest 500 cm^{-1}, which corresponds to ±5 nm at 30 000 cm^{-1}.

(31) (a) Assignment for the UV absorption spectrum of PPh_3 in ethanol:[31b] $\pi \rightarrow \pi^*$ at 3.5×10^4 cm^{-1} ($\epsilon = 1.0 \times 10^3$), $n \rightarrow \pi^*$ at 3.8×10^4 cm^{-1} ($\epsilon = 1.1 \times 10^4$). (b) Shaw, G.; Becconsall, J. K.; Canadine, R. M; Murray, R. *J. Chem. Soc., Chem. Commun.* **1966**, 425.

(32) Kutal, C. *Coord. Chem. Rev.* **1990**, *99*, 213.

Table VIII. Electronic Absorption Spectral Features of Gold Complexes and Ancillary Ligands[a]

complex	band,[b] cm^{-1} (ϵ_{max}, M^{-1} cm^{-1})	assgnt	
PPh_3	3.5×10^4, sh ($1. \times 10^3$)	$\pi \rightarrow \pi^*$	*c* (ref 31), *d*, *e*
	3.8×10^4 (8.5×10^3)	$n \rightarrow \pi^*$	
$Au(PPh_3)Cl$	3.6×10^4, sh ($7. \times 10^2$)	$\pi \rightarrow \pi^*$ (PPh_3)	*d*, *e*
	3.75×10^4 (2.1×10^3)	$n \rightarrow \pi^*$ (PPh_3)	
$Au(PPh_2Et)Cl$	3.65×10^4, sh ($4. \times 10^2$)	$\pi \rightarrow \pi^*$ (PPh_2R)	*d*, *e*
	3.75×10^4 (1.1×10^3)	$n \rightarrow \pi^*$ (PPh_2R)	
PEt_3	no bands below 4.0×10^4		*f* (ref 40)
$Au(PEt_3)Cl$	no bands below 4.0×10^4		*g* (ref 33)
$Au(PMe_3)Cl$	no bands below 4.0×10^4		*g* (ref 33), *d*
$SH(CH_2)_3SH$	no bands below 4.0×10^4		*c* (ref 47)
p-$HS(C_6H_4)CH_3$	3.5×10^4, sh ($6. \times 10^2$)	IL	*h* (ref 34), *d*, *e*
	3.6×10^4, sh ($4. \times 10^2$)	IL	
	4.0×10^4, sh ($7. \times 10^2$)		
$Au(PMe_3)$(*p*-tc) (**12**)	3.2×10^4, sh ($2. \times 10^3$)	LMCT (S → Au)	*d*, *e*
	3.3×10^4, sh ($1. \times 10^3$)	LMCT (S → Au)	
	3.55×10^4, sh ($9. \times 10^3$)	IL (*p*-tc) + other	
	3.85×10^4, sh ($8. \times 10^3$)	IL (*p*-tc) + other	
$Au(PPh_3)$(*p*-tc) (**11**)	3.0×10^4, sh ($1. \times 10^3$)	LMCT (S → Au)	*d*, *e*
	3.25×10^4, sh ($3. \times 10^3$)	LMCT (S → Au)	
	3.5×10^4, sh ($7. \times 10^3$)	IL (*p*-TC) + other	
	3.6×10^4, sh ($8. \times 10^2$)	$\pi \rightarrow \pi^*$ (PPh_3)	
	3.7×10^4, sh ($8. \times 10^3$)	$n \rightarrow \pi^*$ (PPh_3)	
	3.85×10^4, sh ($3. \times 10^3$)	IL (*p*-tc) + other	
$[Au_2$(*p*-tc)$_2$(dpppn)] (**5**)	3.05×10^4, sh ($2. \times 10^3$)	LMCT (S → Au)	*d*, *e*
	3.3×10^4, sh ($6. \times 10^3$)	LMCT (S → Au)	
	3.55×10^4, sh (1.6×10^4)	IL (*p*-TC) + other	
	3.65×10^4, sh ($7. \times 10^2$)	$\pi \rightarrow \pi^*$ (PPh_2R)	
	3.75×10^4, sh (1.0×10^4)	$n \rightarrow \pi^*$ (PPh_2R)	
	3.9×10^4, sh (1.4×10^4)		
$[Au_2$(*p*-tc)$_2$(dppm)] (**1**)	2.8×10^4, sh (3.3×10^3)	LMCT (S → Au)	*d*, *e*
	3.1×10^4, sh ($6. \times 10^3$)	LMCT (S → Au)	
	3.45×10^4, sh (1.5×10^4)	IL (*p*-TC) + other	
	3.6×10^4, sh ($3. \times 10^2$)	$\pi \rightarrow \pi^*$ (PPh_2R)	
	3.7×10^4, sh (1.2×10^4)	$n \rightarrow \pi^*$ (PPh_2R)	
	3.9×10^4, sh (1.4×10^4)		
[Au(dppb)(pdt)Au] (**8**)	2.95×10^4, sh ($2. \times 10^2$)	LMCT (S → Au)	*d*, *e*
	3.2×10^4, sh ($9. \times 10^2$)	LMCT (S → Au)	
	3.55×10^4, sh ($3. \times 10^3$)		
	3.65×10^4, sh ($9. \times 10^2$)	$\pi \rightarrow \pi^*$ (PPh_2R)	
	3.75×10^4, sh ($8. \times 10^2$)	$n \rightarrow \pi^*$ (PPh_2R)	
[Au(dppe)(pdt)Au] (**6**)	2.85×10^4, sh ($5. \times 10^2$)	LMCT (S → Au)	*d*, *e*
	3.1×10^4, sh ($2. \times 10^3$)	LMCT (S → Au)	
	3.55×10^4, sh (1.8×10^4)		
	3.65×10^4, sh ($1. \times 10^3$)	$\pi \rightarrow \pi^*$ (PPh_2R)	
	3.85×10^4, sh (1.6×10^4)	$n \rightarrow \pi^*$ (PPh_2R) + other	

[a] In methylene chloride unless otherwise noted. [b] All spectral bands are reported to the nearest 500 cm^{-1}; sh = shoulder. [c] In ethanol. [d] This work. [e] Spectral band energy and intensity calculated by using a spectral fitting program. [f] Solvent not specified. [g] In acetonitrile. [h] In isooctane.

below 3.9×10^4 cm^{-1} (see Table VIII). Intraligand and charge-transfer transitions involving PMe_3 can be ruled out since these are expected to be at higher energies. (Note that $Au(PMe_3)Cl$ has no absorption bands below 4.0×10^4 cm^{-1}.[33]) The bands at 3.55×10^4 and 3.85×10^4 cm^{-1} likely involve intraligand (IL) transitions on *p*-tc on the basis of the similarities in peak positions.[34] However, since the intensities of these bands are significantly different from that of the free ligand, there may be additional charge-transfer or metal-centered transitions in this region. In contrast, the two lowest energy bands for **12** at 3.2×10^4 and 3.3×10^4 cm^{-1} do not appear to involve any intraligand transitions because there is a large difference in energy ($(2–3) \times 10^3$ cm^{-1}) between these bands and the intraligand (IL) transitions on *p*-tc. Assignment of the two lowest energy bands in **12** as LMCT transitions is discussed in detail below. The spectrum of **11** is qualitatively similar to that of **12** in the region below 3.9×10^4 cm^{-1}, except for the presence of two additional bands at 3.6×10^4 and 3.7×10^4 cm^{-1}, which are assigned as $\pi \rightarrow \pi^*$ and $n \rightarrow \pi^*$ transitions, respectively, on PPh_3.

The same pattern of six bands observed in the mononuclear gold complex **11** also occurs for the open-chain dinuclear complexes **2**–**5** (see Table VIII for assignment of **5**). Thus it is reasonable to assume that assignments for these dinuclear complexes are the same as those for the mononuclear complexes. Since ligand-centered transitions were previously ruled out for the two lowest energy bands (vide supra), the most likely possibilities are metal-centered or charge-transfer transitions. For mononuclear gold(I) phosphine complexes, metal-centered $d \rightarrow s$ or $d \rightarrow p$ transitions generally occur higher than ca. 4×10^4 cm^{-1}.[35] For gold(I) dinuclear complexes which have a gold(I)–gold(I) bond, metal-centered transitions occur at lower energy due to destabilization of the highest occupied d orbital (which becomes σ antibonding). Consequently metal-centered $d\sigma^* \rightarrow s$ or $d\sigma^* \rightarrow p$ transitions have been assigned in the region (2.9–3.9) $\times 10^4$ cm^{-1}.[36] Although the solid-state structures of **4** and **5** reveal intermolecular Au–Au interactions, there is no evidence that these weak interactions are maintained in solution, e.g. no concentration-dependent behavior is observed. In addition the fact that the spectra for dinuclear gold complexes **2**–**5** are very

(33) (a) $Au(PMe_3)Cl$ has an absorption band at 4.28×10^4 cm^{-1} in CH_3CN solution which has been assigned as an MLCT (Au → P) transition.[33b] (b) Savas, M. M.; Mason, W. R. *Inorg. Chem.* **1987**, *26*, 301.

(34) *Organic Electronic Spectral Data*; Kamlet, M. J., Ed.; John Wiley and Sons: New York, 1946–1952, p 153. The UV spectrum of *p*-tc in isooctane solution is very similar to the results of the spectral fit in CH_2Cl_2: 3.5×10^4 cm^{-1} ($\epsilon = 6 \times 10^2$), 3.6×10^4 cm^{-1} ($\epsilon = 6 \times 10^2$), 4.2×10^4 cm^{-1} ($\epsilon = 9 \times 10^3$).

(35) (a) See ref 33b. (b) Jaw, H.-R. C.; Mason, W. R. *Inorg. Chem.* **1989**, *28*, 4370.

(36) (a) Jaw, H.-R. C.; Savas, M. M.; Mason, W. R. *Inorg. Chem.* **1989**, *28*, 4366. (b) King, C.; Wang, J.-C.; Khan, Md. N. I.; Fackler, J. P., Jr. *Inorg. Chem.* **1989**, *28*, 2145. (c) Jaw, H.-R. C.; Savas, M. M.; Rogers, R. D.; Mason, W. R. *Inorg. Chem.* **1989**, *28*, 1028. (d) von Ludwig, W.; Meyer, W. *Helv. Chim. Acta* **1982**, *65*, 934.

similar to the spectrum for mononuclear complex **11** suggests that Au–Au interactions are not responsible for the two lowest energy bands at 3.2×10^4 and 3.0×10^4 cm^{-1}.

The data are most consistent with assignment of the two lowest energy bands as charge-transfer transitions involving the sulfur ligand. The electronic absorption spectra of **4** and **5** were measured in CH_2Cl_2, THF, and CH_3CN. Analysis of the derivative spectra reveals that the bands at 3.2×10^4 and 3.0×10^4 cm^{-1} shift to higher energy with increasing solvent polarity.[37] For example, in **5** the two lowest energy bands blue-shift by ca. 625 cm^{-1} from THF to CH_2Cl_2 and ca. 125 cm^{-1} from CH_2Cl_2 to CH_3CN. The observed solvatochromism is consistent with a charge-transfer transition that decreases the size of the molecular dipole moment.[37] From a consideration of Pauling's electronegativity values, the ground-state dipole for linear P–Au–S complexes is likely to be oriented with negative charge on the thiolate ligand.[38] Thus a S → Au CT excited state would have a smaller dipole moment and would be expected to blue-shift with increasing solvent polarity.

Ligand-to-metal CT transitions are often distinguished from MLCT's by changing the electron-donating properties of the substituents on ligands.[37,39] The analogue of **2** was prepared with the more electron-withdrawing 3,4-dichlorobenzenethiolate substituted for *p*-tc. Examination of the derivative spectrum for [Au_2(3,4-dichlorobenzenethiolate)$_2$(dppe)] (**2′**) reveals that the two lowest energy bands are blue shifted compared to those for **2**. This is consistent with an LMCT since 3,4-dichlorobenzenethiolate is harder to oxidize than *p*-tc. Alternatively, a red shift is expected for an LMCT (S → Au) transition if the trans phosphine ligand is made more electron withdrawing. This is indeed observed: compare **12** to **11** (Table VIII). Finally, Brown et al. studied the electronic spectra of mononuclear gold(I) complexes with thiolate and phosphine ligands.[40] They assigned bands at ca. 360 and 290 nm (2.77×10^4 and 3.45×10^4 cm^{-1}) as S → Au charge-transfer transitions on the basis of UV–visible and CD spectra and SCF–MO calculations.

There are six bands below 4.0×10^4 cm^{-1} in the absorbance spectrum of **1**, just as there are for **2–5**. However, the two lowest energy bands for **1**, at 2.8×10^4 and 3.1×10^4 cm^{-1} are red-shifted compared to the two lowest energy bands for **5** (compare Figures 3 and 4). This difference is visually striking: **1** is yellow in solution while **2–5** are colorless. Spectra of **1** obtained in different solvents reveal the same solvent dependence as seen for **5**; i.e., the two lowest energy bands blue-shift with increasing solvent polarity. (There is a 600-cm^{-1} blue shift from THF to CH_2Cl_2 and a 200-cm^{-1} blue shift from CH_2Cl_2 to CH_3CN.) The result of substitution of *p*-tc by 3,4-dichlorobenzenethiolate is also striking. The complex [Au_2(3,4-dichlorobenzenethiolate)$_2$(dppm)] (**1′**) is colorless in solution, and examination of the derivative spectrum reveals that the two lowest energy bands blue-shift relative to those for **1** (e.g., the lowest energy band shifts by ca. 1000 cm^{-1} to 2.9×10^4 cm^{-1}). Thus the two lowest energy absorption bands for **1** are also assigned as LMCT transitions.

Why are the LMCT (S → Au) transitions at lower energy in **1** than in the other open-chain complexes, **2–5**? An obvious structural difference between **1** and **2–5** is the number of methylene groups (*n*) between phosphorus atoms. Variation in the phosphine electronic properties as *n* increases is not expected to be large.[41]

Scheme I

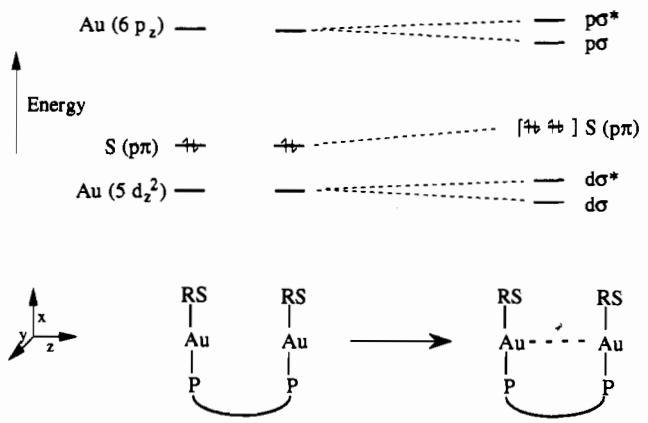

Indeed, the ^{31}P chemical shifts for **1–5** occur within a narrow range (see Table I). Thus another factor is likely responsible for the red shift resulting in the yellow color of **1**.

In other examples of d^{10} metal thiolate complexes, an increase in coordination number from linear to trigonal geometry has been observed to cause a red shift in the LMCT transitions.[42] This has been rationalized on the basis of destabilization of sulfur (p) orbitals due to increased ligand–ligand repulsion.[37] Since there is not an excess of ligand present in solutions of **1**, a three-coordinate complex is unlikely to be responsible for the red shift. Furthermore, if an increase in coordination was responsible for the red shift, then it should be possible to induce a similar red shift in one of the other members of the open-chain series by adding a phosphine or thiolate ligand. However, addition of 2.3 equiv of dpppn to a 1.1×10^{-4} M CH_2Cl_2 solution of **5** causes no change in the UV–visible spectrum below 3.4×10^4 cm^{-1} (dpppn absorbs at $>3.4 \times 10^4$ cm^{-1}). Similarly, addition of 2 equiv of either protonated or deprotonated *p*-tc does not change the UV–visible spectrum of **5**.

Increased repulsion between the lone pairs on sulfur could also occur as a result of the close approach of two gold atoms. Analysis of solid-state structural data (vide supra) suggests that **1** is a likely candidate for an intramolecular gold–gold interaction since there is only one methylene group in the bridging bis(phosphine) ligand. In addition to destabilizing the sulfur orbitals, gold–gold interactions are expected to destabilize the filled 5d$_{z^2}$ orbital that becomes σ^* and to stabilize the empty 6p orbital that becomes σ bonding.[43] These points are summarized in a one-electron MO diagram shown in Scheme I, where the S($p\pi$) orbital is the HOMO.[44] The net effect is that an increase in gold–gold interaction (going from left to right in Scheme I) causes a S → Au charge-transfer transition to red-shift. This analysis leads us to suggest that in solution, complex **1** displays a significantly larger gold–gold interaction than does **5**. (Variable-temperature NMR studies (vide infra) and electrochemical experiments are also consistent with the presence of a gold–gold interaction for **1** but not for **5**.[45])

The presence of a gold–gold bond in **1** may be expected to cause additional changes in the electronic spectrum on the basis of studies by Mason et al. on related dinuclear gold complexes.[35b] The lowest energy transition for [Au_2(LL)$_2$](ClO$_4$)$_2$ (LL = dmpm

(37) Lever, A. B. P. *Inorganic Electronic Spectroscopy*, 2nd ed.; Elsevier: Amsterdam, 1984; pp 206–211. Reichardt parameters (E_T) for selected solvents: THF, E_T = 37.4; CH_2Cl_2, E_T = 41.1; CH_3CN, E_T = 46.0.

(38) Pauling, L. *The Nature of the Chemical Bond*, 3rd ed.; Cornell University Press: Ithaca, NY, 1960; p 93.

(39) Geoffroy, G. L.; Wrighton, M. S. *Organometallic Photochemistry*; Academic Press: New York, 1979; p 17.

(40) Brown, D. H.; McKinlay, G.; Smith, W. E. *J. Chem. Soc., Dalton Trans.* **1977**, 1874.

(41) Using Tolman's substituent additivity rule, the following electronic properties (χ_i) can be calculated for monodentate tertiary phosphines: P(Ph)$_2$Me, 11.2; P(Ph)$_2$(Et), 10.4; P(Ph)$_2$(*i*-Pr), 9.6; P(Ph)$_2$(*n*-Bu), 10.0. See: Tolman, C. A. *J. Am. Chem. Soc.* **1970**, *92*, 2953.

(42) (a) The lowest energy transitions in Hg(II) thiolate complexes, assigned as LMCTs, red-shift upon changing from two-coordinate linear to trigonal planar geometry: Watton, S. P.; Wright, J. G.; MacDonnell, F. M.; Bryson, J. W.; Sabat, M.; O'Halloran, T. V. *J. Am. Chem. Soc.* **1990**, *112*, 2824. (b) [Cu(SC$_6$H$_5$)$_2$]$^-$ is white while [Cu(SC$_6$H$_5$)$_3$]$^{2-}$ is orange-red: Coucouvanis, D.; Murphy, C. N.; Kanodia, S. K. *Inorg. Chem.* **1980**, *19*, 2993.

(43) (a) See ref 36b. (b) See ref 36c. (c) Balch, A.; Catalano, V. J. *Inorg. Chem.* **1991**, *30*, 1302.

(44) The real situation is probably more complicated because of mixing of gold and sulfur orbitals that have the same symmetry and are close in energy. All orbitals below the pair of electrons shown in Scheme I are filled.

(45) Turmel, C.; Jian, T.; Wei, G.; Bruce, A.; Bruce, M. Unpublished results.

or dmpe) in CH_3CN has been assigned as a metal-centered $d\sigma^* \rightarrow p\sigma$ transition. These transitions occur near 3.1×10^4 cm^{-1} with extinction coefficients between 200 and 900. Thus, an intramolecular gold–gold bond may be expected to give rise to an additional metal-centered band or bands in the same region as the LMCT transitions in **1**. There are several pieces of evidence that are consistent with the presence of an additional band below 3.0×10^4 cm^{-1}. First the extinction coefficient of the band at 2.8×10^4 cm^{-1} for **1** is ca. 1.5 times greater than that of the band at 3.05×10^4 cm^{-1} for **5**. Second, results of spectral fits indicate that the lowest energy band is significantly broader in **1** than in **5** (compare Figures 4iii and 3iii).[46]

The results of spectral fits for complexes **8** and **6** are presented in Table VIII (also in Figures B and A, supplementary material). The two highest energy bands are assigned as IL transitions on the phosphine ligand in analogy to the cases for **1** and **5**. There is insufficient information to assign the band at 3.55×10^4 cm^{-1}. However an IL transition on the thiolate ligand is unlikely because propanedithiol does not absorb below 40 000 cm^{-1}.[47] Assignment of the two lowest energy bands as LMCT (S → Au) transitions is based on a comparison of **8** to **5**. An LMCT (S → Au) transition should be at lower energy for an aliphatic thiolate than for an aromatic thiolate and this is indeed the case. The two lowest energy bands for **8** are each red-shifted by ca. 1000 cm^{-1} (10 nm) relative to the corresponding bands for **5**.

Results of spectral fits indicate that the two lowest energy LMCT (S → Au) transitions in **6** are red-shifted by 1000 cm^{-1} relative to those in **8**. Although the magnitude of the red shift is smaller, this is the same trend observed in the open-chain series; the LMCT transitions are red-shifted for complexes with the shorter bis(phosphine) ligand backbones relative to the longer ones. The difference between **6** and **8** is not expected to be caused by differences in the electronic properties of the phosphine ligand (vide supra). Therefore, it appears likely that the two lowest energy bands are red-shifted in **6** vs **8** for a similar reason as was suggested for **1** vs **5**, i.e. increased gold–gold interactions which destabilize the sulfur (p) orbital.

NMR Studies. The ^{31}P chemical shifts for complexes **1–10** occur within a narrow range (28–37 ppm) and in a region of the spectrum that is typical for gold(I) coordinated to an alkyl- or arylphosphine.[48] The general trend within each series, **1–5** and **6–9**, is that as the number of connecting carbons (n) in the phosphine ligand backbone increases, the phosphorus chemical shift becomes more positive. The exceptions occur for **2** and **6** with $n = 2$, for which the ^{31}P chemical shifts are 5–6 ppm more positive than for **3** and **7**, with $n = 3$. This trend is also observed for the free phosphines and most likely reflects small variations in dihedral or bond angles at phosphorus as the length of the alkyl backbone changes.[48a] Comparison of coordination chemical shifts ($\Delta = \delta_{complex} - \delta_{free}$; see Table I) is also informative. This parameter is often used to evaluate ring contributions to the chemical shift for phosphorus nuclei involved in a chelate ring.[49] It has recently been demonstrated that the ring effect disappears in larger than six-membered rings.[50] For **1–9**, the small variation in Δ (46.6–52.2) confirms the absence of any ring effect for bis(phosphines) bridging two metals and indicates that the phosphorus environments are very similar in the open-chain and cyclic complexes. This is also consistent with conclusions from UV–visible experiments; i.e., changing the bis(phosphine) ligand does little to perturb the electronic absorption spectra (below 4.0×10^4 cm^{-1}).

At room temperature, each complex exhibits a singlet in the $^{31}P\{^1H\}$ NMR spectrum, consistent with the equivalence of all phosphorus atoms in solution. The signals are sharp (ca. 3 Hz) for all complexes except **1**, which has a line width of ca. 30 Hz. Variable-temperature NMR (VT-NMR) experiments were carried out in CD_2Cl_2 solution for one mononuclear gold complex (**11**), two open-chain complexes (**1**, **4**), and two cyclic complexes (**6**, **9**). Complex **1** was investigated by ^{31}P and ^1H VT-NMR, and the others were investigated by ^{31}P VT-NMR only. Phosphorus-31 NMR spectra obtained from −80 to +20 °C are plotted in Figure 5 for **1** and **4**. The dinuclear complex **4** and the mononuclear complex **11** each display a singlet in the $^{31}P\{^1H\}$ NMR spectra at all temperatures, which broadens only slightly and shifts upfield by <1 ppm as the temperature decreases (see Figure 5A for spectra of **4**). In contrast, two temperature-dependent processes are observed for **1** (Figure 5B). At −80 °C the spectrum consists of two broad signals of unequal intensity at 30.1 and 32.2 ppm. In addition there are some very weak, broad peaks near 34 and 36 ppm. At −60 °C the signals at 30.1 and 32.2 ppm coalesce to one broad peak at 30.4 ppm, which decreases in line width until the temperature reaches −20 °C, where the line width is ca. 6 Hz. Upon a further increase in the temperature, the peak broadens again and the weak resonances near 35 ppm are no longer visible. The same result was obtained for solutions of **1** that differed in concentration by a factor of 2 (0.07 and 0.035 M).

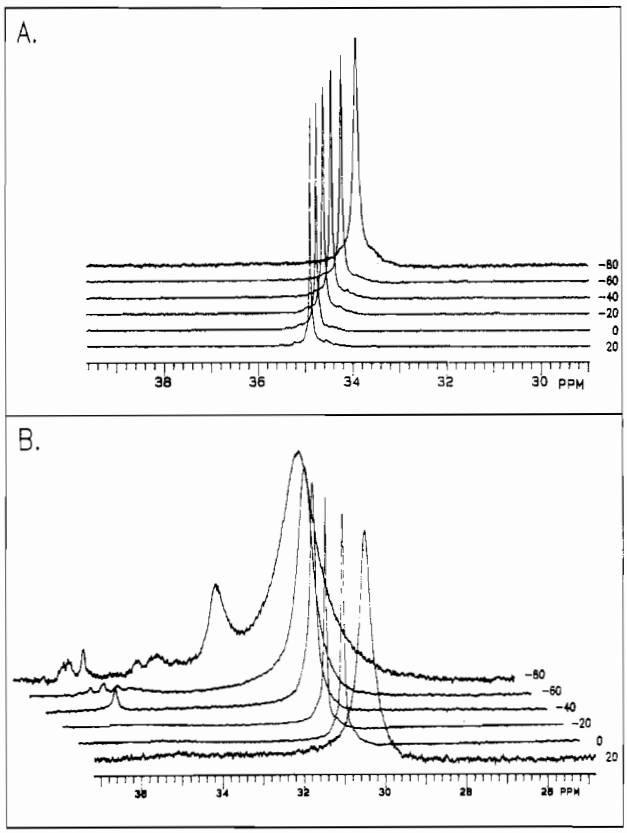

Figure 5. Variable-temperature ^{31}P NMR spectra in CD_2Cl_2 from −80 to +20 °C as indicated: (A) $[Au_2(p\text{-tc})_2(dppb)]$ (**4**), no offset; (B) $[Au_2(p\text{-tc})_2(dppm)]$ (**1**), spectra offset for clarity.

The variable-temperature ^1H NMR spectra for **1** also reveal similar temperature-dependent processes. For example, at −80 °C there are two equal-intensity triplets for the methylene protons on the bis(phosphine) at 4.04 and 3.75 ppm and a very weak, broad signal near 4.8 ppm. At −40 °C the two triplets coalesce and at 0 °C there is one sharp triplet centered at 3.9 ppm (J_{PH} = 11 Hz). At room temperature, the triplet is broader and the weak signal near 4.8 ppm has disappeared.

Line shape analysis for the major set of peaks at 30.1 and 32.2 ppm in the ^{31}P NMR of **1** was carried out using a coalescence temperature of −60 °C and a peak separation at the low

(46) The broadness may also be due to splitting of the sulfur (HOMO) orbitals.
(47) *Handbook of Data on Organic Compounds*, 2nd ed.; Weast, R. C., Grasselli, J. G., Eds.; CRC Press: Boca Raton, FL, 1988; p 3650.
(48) (a) Pregosin, P. S. In *Phosphorus-31 NMR Spectroscopy in Stereochemical Analysis*; Verkade, J. G., Quin, L. D., Eds.; VCR: Deerfield Beach, FL, 1987. (b) Al-Baker, S.; Hill, W. E.; McAuliffe, C. A. *J. Chem. Soc., Dalton Trans.* **1985**, 2655. (c) See ref 13.
(49) Garrou, P. E. *Chem. Rev.* **1981**, *81*, 229.
(50) Lindner, E.; Fawzi, R.; Mayer, H. A.; Eichele, K.; Hiller, W. *Organometallics* **1992**, *11*, 1033.

temperature limit of 170 Hz.[51] The calculated value for the activation energy is 10 ± 1 kcal/mol.[52] An activation energy of ca. 10 kcal/mol is consistent with several processes; two possibilities will be considered. Rotations about C–P single bonds can occur with activation energies near 10 kcal/mol.[53] However, the absence of a temperature-dependent process for **4** suggests that C–P bond rotations in the open-chain complexes have much lower activation energies. Alternatively, a fluxional process involving interconversion of gold(I)–gold(I) bonded and nonbonded isomers of **1** may be responsible for the observed temperature dependence. Preliminary MM2 calculations indicate that a cis conformation of **1** is ≈8 kcal/mol higher in energy than a trans conformation.[54] Thus, formation of an intramolecular gold(I)–gold(I) bond would decrease the energy of the cis conformation by ≈10 kcal/mol[6a,8] and yield an isomer of **1** that is close in energy to the trans conformation (within 1–2 kcal/mol). In the fast-exchange region, interconversion of trans nonbonded and cis bonded isomers would lead to a single broadened resonance. This fluxional process is also consistent with UV–visible results for **1** (vide supra), which suggest that an intramolecular gold(I)–gold(I) bond is responsible for the red shift in the two lowest energy LMCT transitions.

A second temperature-dependent process is responsible for the increase in line widths from –20 to +20 °C in the ^{31}P and ^{1}H NMR spectra of **1**. It is likely that an acid–base equilibrium is involved since addition of small amounts of aqueous HCl (pH 3) to a CD_2Cl_2 solution of **1** at room temperature essentially reproduces the 0 °C ^{1}H NMR spectrum; i.e., the triplet for the dppm ligand (3.9 ppm) sharpens and a weak peak at 4.75 ppm appears. The ^{1}H NMR spectrum is also concentration dependent; at 3 mM, the triplet is at 3.77 ppm, while at 20 mM, it is significantly broadened and appears at 3.87 ppm. The origin of the higher temperature-dependent process, the acid sensitivity, and the concentration dependence are currently under investigation. However, it is important to note that the UV–visible spectra of **1** are not altered by decreasing the temperature to 0 °C, adding small amounts of HCl, or varying the concentration of **1**.

Variable-temperature $^{31}P\{^{1}H\}$ NMR experiments on the cyclic complexes **6** and **9** are similar to those for **1** with the exception that only one temperature-dependent process is observed for each complex. At –80 °C, the ^{31}P NMR spectrum of **9** displays two broad signals of unequal intensity at 33.2 and 35.8 ppm. These peaks coalesce to a single peak at –60 °C, which decreases smoothly in line width as the temperature increases. The activation energy for this dynamic process (determined by line shape analysis) is 10 ± 1 kcal/mol.[52] The ^{31}P NMR spectrum of **6** at –80 °C is extremely broad, and an increase in temperature results in a steady decrease in line width. (A coalescence point was not determined.) Since complexes **6** and **9** are 11- and 13-membered rings, respectively, the dynamic processes may originate from ring inversion. Activation energies for ring inversion vary widely and depend on the ring size, the substituents, and the degree of strain in the ground state. However, 9-membered or larger carbocyclic rings (also containing O, N, or S) that are highly nonplanar generally have large conformational barriers (>15 kcal/mol).[55] On the basis of the similarities in $\Delta G^{\ddagger}$ for **1** and **9**, a likely alternative is that the dynamic process originates from equilibria between gold(I)–gold(I) bonded and nonbonded conformations.

Summary. *Intermolecular* gold–gold interactions occur in the solid-state structures of the two largest, open-chain molecules **4** and **5** [Au–Au = 3.094(1) and 3.200(1) Å, respectively]. All of the open-chain and cyclic dinuclear gold complexes are white, with the exception of **1**, which is yellow. The lowest energy electronic transitions for complexes **1–9**, **11**, and **12** are assigned as LMCT (S → Au) transitions. The absorption spectra of the open-chain complexes **2–5** (in which *n* successively increases from 2 to 5) are nearly superimposable. However in complex **1**, where *n* = 1, the lowest energy band is significantly red shifted (by 2.5 × 10^3 cm^{-1} relative to that of **5**). In the cyclic dinuclear gold(I) complexes a similar trend is found: the lowest energy band in **6** is red-shifted by 1.0 × 10^3 cm^{-1} relative to that of **8**. We hypothesize that two factors contribute to the red shifts: gold(I)–gold(I) interactions and repulsive interactions between sulfur-centered HOMO orbitals. Variable-temperature ^{1}H and ^{31}P NMR studies indicate the presence of fluxional processes for complexes **1**, **6**, and **9** but not for **4**. Together, the UV–visible and variable-temperature NMR studies suggest that in solutions of **1** and **6–9** there are equilibria between *intramolecular* gold–gold bonded and nonbonded conformational isomers.

The results of this study may have biological implications for the neutral phosphine gold(I) thiolate complexes used in the treatment of rheumatoid arthritis. It is well established that gold(I) phosphines bind to cysteine sulfur in proteins. Our study suggests that it may be possible for two Au–cysteine sites to interact via gold–gold bonds but only if the two sites are closely situated. Thus, knowledge of a protein's three-dimensional structure may provide a way of evaluating possible candidates for gold(I)–gold(I) interactions. In addition, gold–gold interactions may promote gold redox chemistry since interacting transition metals can alter redox behavior.[56] A lowering of the oxidation potential, for example, may lead to the generation of toxic Au(III) complexes. Another possible site of redox activity is a disulfide bridge, where Au(I) → Au(III) oxidation may couple with disulfide reduction. Studies are now underway to evaluate these possibilities. We are also investigating gold(I)–gold(I) interactions by EXAFS spectroscopy, emission spectroscopy, and cyclic voltammetry. These studies will be reported in forthcoming papers.

Acknowledgment. A.E.B. and M.R.M.B. gratefully acknowledge financial support from the National Institutes of Health (Grant AR39858) and the University of Maine BRSG funds. We thank Dr. R. Anderegg (Glaxo, Inc.) for kindly providing FAB-MS data. We are grateful to Professors J. P. Fackler, Jr., J. Nagle, G. Parkin, and J. L. Templeton for helpful discussions. Private communication of unpublished results from Professor Fackler is also acknowledged. Mr. L. Lester (at UM) is acknowledged for technical assistance.

Supplementary Material Available: Absorption and derivative spectra and spectral fits for **6**, **8**, and **11** (Figures A–C) and tables listing complete details of the structure determination, H atom coordinates and isotropic displacement parameters, anisotropic temperature parameters, and bond distances and angles for **4** and **5** (23 pages). Ordering information is given on any current masthead page.

(51) Binsch, G. In *Dynamic Nuclear Magnetic Resonance Spectroscopy*; Jackman, L. M., Cotton, F. A., Eds.; Academic Press: New York, 1975; p 49.

(52) (a) Equal populations of different ^{31}P sites can display different intensities due to different T_1 values and NOEs.[48a] However, line shape analysis was also carried out using the graphical method of Shanan-Atidi and Bar-Eli for unequal population of sites.[52b] By using this method, the calculated $\Delta G^{\ddagger}$ is also 10 kcal/mol. (b) Shanan-Atidi, H.; Bar-Eli, K. H. *J. Phys. Chem.* **1970**, *74*, 961.

(53) Schmidbaur, H.; Deschler, U.; Milewski-Mahrla, B. *Chem. Ber.* **1983**, *116*, 1393.

(54) Hyperchem molecular modeling software by Autodesk, 2320 Marinship Way, Sausalito, CA 94965.

(55) See ref 51, p 604.

(56) (a) Downard, A. J.; Honey, G. E.; Phillips, L. F.; Steel, P. J. *Inorg. Chem.* **1991**, *30*, 2260. (b) Auburn, P. R.; Lever, A. B. P. *Inorg. Chem.* **1990**, *29*, 2551. (c) Koley, A. P.; Purohit, S.; Ghosh, S.; Prasa, L. S.; Manoharan, P. T. *J. Chem. Soc., Dalton Trans.* **1988**, 2607.